THEORY OF BERNSTEIN WAVES COUPLING WITH LOOP ANTENNAS

M. Brambilla

IPP 5/15

April 1987

MAX-PLANCK-INSTITUT FÜR PLASMAPHYSIK

8046 GARCHING BEI MÜNCHEN

MAX-PLANCK-INSTITUT FÜR PLASMAPHYSIK

GARCHING BEI MÜNCHEN

THEORY OF BERNSTEIN WAVES COUPLING WITH LOOP ANTENNAS

M. Brambilla

IPP 5/15 April 1987

Die nachstehende Arbeit wurde im Rahmen des Vertrages zwischen dem Max-Planck-Institut für Plasmaphysik und der Europäischen Atomgemeinschaft über die Zusammenarbeit auf dem Gebiete der Plasmaphysik durchgeführt.

THEORY OF BERNSTEIN WAVES COUPLING WITH LOOP ANTENNAS

M. Brambilla

IPP 5/15

Abstract

We present a fully three-dimensional theory of antenna coupling to Ion Bernstein Waves near the first harmonic of the ion cyclotron resonance in tokamak plasmas. The boundary conditions in vacuum are solved analytically for arbitrary orientation of the antenna and Faraday screen conductors. The wave equations in the plasma, which include Finite Larmor Radius and finite electron inertia effects, cyclotron and harmonic damping by the ions, and Landau and collisional damping by the electrons, are solved numerically using a Finite Elements discretisation with cubic Hermite interpolating functions.

Applications to Alcator C give reasonably good agreement between the calculated and measured radiation resistance in the range in which efficient heating is observed; outside this range the calculated resistance is lower than the experimental one. In general, the coupling efficiency is found to be very sensitive to the edge plasma density, good coupling requiring a low density plasma layer in the vicinity of the Faraday screen. Coupling also improves with increasing scrape-off ion temperature, and is appreciably better for antisymmetric than for symmetric toroidal current distributions in the antenna.

1. - Introduction.

Plasma heating with ion Bernstein Waves has been proposed as a viable alternative to Fast Wave heating in the ion cyclotron frequency domain [1]-[4]. Several moderate power experiments have shown promising efficiency [5] - [13]; for a recent review and additional references, cfr. [14]. The theory of antennas designed for Bernstein wave launching, however, has received relatively little attention. Analytic estimates of the plasma surface impedance for BW have been made by Puri [15]. Skiff et al. [16] have considered the parasitic excitation of BW due to density gradients in a FW launching experiment, using an expansion valid for steep gradients. The evaluation of direct launching of BW, however, requires the numerical solution of the full wave equations in the plasma. This has been done in a two dimensional approximation by Sy et al. [17]. In this paper we present a fully three dimensional code for the same purpose.

A BW antenna must be rotated by $\pi/2$ with respect to a conventional FW antenna, so that the current flows along the static magnetic field, while the Faraday shield screens the poloidal electric field of the wave. This configuration rules out two approximations which considerably simplify the theoretical description of FW launching in the same frequency range, namely that the component of the h.f. electric field E_z parallel to the static magnetic field vanishes everywhere in the plasma, and that, as a consequence, reflection and trasmission of a plane wave at the plasma boundary can be described by a scalar surface impedance, $Z_F = E_y(0)/B_z(0)$. On the contrary, launching Bernstein waves requires a finite $E_z(0)$; thus the full tensor surface impedance must be evaluated, taking into account both finite Larmor radius (FLR) and finite electron inertia terms in the wave equations in the plasma.

The geometry we have adopted for this purpose is similar to the one used for most FW coupling calculations [18-22]. The real configuration is approximated by a slab model: the static magnetic field is in the z direction, and its intensity, as well as the plasma parameters, vary only in the x direction. In other words, Cartesian coordinates (x, y, z) simulate the radial, poloidal and toroidal directions, respectively, of a tokamak, but curvature and shear of the magnetic field lines are neglected. The wave field is decomposed in a double Fourier sum

$$\vec{E}(x,y,z,t) = \sum_{n_z} \sum_{n_y} \vec{E}(n_z, n_y, x) e^{i(k_z z + k_y y - \omega t)} \qquad (1)$$

The toroidal and poloidal wavenumbers $n_z = ck_z/\omega$ and $n_y = ck_y/\omega$ are for convenience

discretised as appropriate in the equivalent toroidal problem:

$$\begin{aligned} n_z &= \frac{n_\phi}{\left(\frac{\omega}{c} R_T\right)} \qquad && (-\infty < n_\phi < \infty) \\ n_y &= \frac{m_\theta}{\left(\frac{\omega}{c} a\right)} \qquad && (-\infty < m_\theta < \infty) \end{aligned} \tag{2}$$

where n_ϕ and m_θ are integers, and R_T and a are the major and minor radius of the plasma, respectively. In the simplified slab geometry adopted, each partial wave can be treated separately, since both the fields and the power flux are additive.

The solution in vacuum is presented in the next section. The circumstance that this solution can be obtained analytically for an arbitrary orientation of the antenna and Faraday conductors with respect to the direction of the static magnetic field will be useful to extend the present work in several directions. In the first place, a selfconsistent evaluation of the current distribution $J^a(y,z)$ in the antenna using the variational formulation of Teilhaber and Jacquinot [22] becomes possible without much additional effort; here however it was not attempted, and $J^a(y,z)$ is supposed known. Secondly, the same method can be applied to treat BW coupling using waveguides, one of the most attractive features of this heating scheme. Applications are possible to situations in which the conductors cannot be easily aligned with the static magnetic fields, as in Stellarators. Finally, the code can be used to investigate parasitic effects in conventional FW coupling, such as density gradient coupling to the BW [17], or surface absorption due to the presence of the Lower Hybrid resonance in the scrape-off plasma [23]. Some of these applications will be presented in forthcoming reports.

The main originality of this work lies in the treatment of propagation in the plasma, which is presented in Section 3. To describe Bernstein waves, FLR effects and finite electron inertia have to be taken into account, so that a sixth order differential system of equations has to be solved. Of the three waves formally described by this system, however, only two are physically meaningful, namely the fast wave, and a shorter wavelength mode whose dispersion characteristics depend sensitively on the plasma parameters. In order to follow the transformation of this mode [14] from a cold plasma wave (the shear Alfven wave or its kinetic modification) near the plasma edge to the BW proper in the hotter plasma core, while rejecting the spurious solution of the wave equations, a finite element discretisation with cubic Hermite interpolation functions [24] has been used.

The solution is made unique by assuming that outward radiation conditions can be imposed at sufficiently high density in the plasma. This requires that the plasma is sufficiently large and lossy to exclude the excitation of global eigenmodes. It can easily be relaxed in principle, and we have actually done it to test wether the code can be

applied to situations where this assumption is justified for the Bernstein waves, but does not hold for the Fast Wave. It turns out that BW coupling is little affected if a large standing wave ratio is assumed for the Fast Wave. It should be noted however that the slab shearless model is often inadequate to describe the plasma as a whole.

Some applications of our code to the simulation of the experimental results obtained in Alcator C [13] are presented in Section 4. Agreement is on the whole sarisfactory, although not all details can be reproduced. According to the code, Bernstein waves can be efficiently launched only if the first harmonic cyclotron resonance is locate behind the antenna, and sufficiently close to it, so that BW near the plasma edge have a relatively large wavelength. In this range, which coincides with the domain in which efficient heating is observed in the experiment, we find a radiation resistance comparable to the one measured. On the other hand the radiation resistance predicted far from the region of efficient heating is appreciably smaller than the one measured, even when collisional damping is taken into account.

We also find that the radiation resistance of a BW antenna is very sensitive to the value of the density, and to a lesser extent of the temperature, near the plasma edge. For good coupling, the plasma in the immediate vicinity of the antenna must have a sufficiently low beta, $\beta << m_e/m_i$. We show that the most important parameter in this respect is the edge plasma density: when it is large, the electrons screen efficiently the component of the wave electric field parallel to the static magnetic field, which is essential for coupling to slow plasma waves. This suggests that protecting the antenna with lateral auxiliary limiters protruding somewhat into the scrape-off plasma might considerably improve coupling. The value of the edge density gradient on the other hand has no influence on the coupling within the range explored. An increase in the scrape-off ion temperature improves matching by increasing the BW wavelength. We also find that a quadrupole T-antenna with central feeder and shorts at the ends is better matched than a dipole one with feeders at the ends and short in the middle.

discretised as appropriate in the equivalent toroidal problem:

$$\begin{aligned} n_z &= \frac{n_\phi}{\left(\frac{\omega}{c} R_T\right)} \qquad && (-\infty < n_\phi < \infty) \\ n_y &= \frac{m_\theta}{\left(\frac{\omega}{c} a\right)} \qquad && (-\infty < m_\theta < \infty) \end{aligned} \tag{2}$$

where n_ϕ and m_θ are integers, and R_T and a are the major and minor radius of the plasma, respectively. In the simplified slab geometry adopted, each partial wave can be treated separately, since both the fields and the power flux are additive.

The solution in vacuum is presented in the next section. The circumstance that this solution can be obtained analytically for an arbitrary orientation of the antenna and Faraday conductors with respect to the direction of the static magnetic field will be useful to extend the present work in several directions. In the first place, a selfconsistent evaluation of the current distribution $J^a(y,z)$ in the antenna using the variational formulation of Teilhaber and Jacquinot [22] becomes possible without much additional effort; here however it was not attempted, and $J^a(y,z)$ is supposed known. Secondly, the same method can be applied to treat BW coupling using waveguides, one of the most attractive features of this heating scheme. Applications are possible to situations in which the conductors cannot be easily aligned with the static magnetic fields, as in Stellarators. Finally, the code can be used to investigate parasitic effects in conventional FW coupling, such as density gradient coupling to the BW [17], or surface absorption due to the presence of the Lower Hybrid resonance in the scrape-off plasma [23]. Some of these applications will be presented in forthcoming reports.

The main originality of this work lies in the treatment of propagation in the plasma, which is presented in Section 3. To describe Bernstein waves, FLR effects and finite electron inertia have to be taken into account, so that a sixth order differential system of equations has to be solved. Of the three waves formally described by this system, however, only two are physically meaningful, namely the fast wave, and a shorter wavelength mode whose dispersion characteristics depend sensitively on the plasma parameters. In order to follow the transformation of this mode [14] from a cold plasma wave (the shear Alfven wave or its kinetic modification) near the plasma edge to the BW proper in the hotter plasma core, while rejecting the spurious solution of the wave equations, a finite element discretisation with cubic Hermite interpolation functions [24] has been used.

The solution is made unique by assuming that outward radiation conditions can be imposed at sufficiently high density in the plasma. This requires that the plasma is sufficiently large and lossy to exclude the excitation of global eigenmodes. It can easily be relaxed in principle, and we have actually done it to test wether the code can be

applied to situations where this assumption is justified for the Bernstein waves, but does not hold for the Fast Wave. It turns out that BW coupling is little affected if a large standing wave ratio is assumed for the Fast Wave. It should be noted however that the slab shearless model is often inadequate to describe the plasma as a whole.

Some applications of our code to the simulation of the experimental results obtained in Alcator C [13] are presented in Section 4. Agreement is on the whole sarisfactory, although not all details can be reproduced. According to the code, Bernstein waves can be efficiently launched only if the first harmonic cyclotron resonance is locate behind the antenna, and sufficiently close to it, so that BW near the plasma edge have a relatively large wavelength. In this range, which coincides with the domain in which efficient heating is observed in the experiment, we find a radiation resistance comparable to the one measured. On the other hand the radiation resistance predicted far from the region of efficient heating is appreciably smaller than the one measured, even when collisional damping is taken into account.

We also find that the radiation resistance of a BW antenna is very sensitive to the value of the density, and to a lesser extent of the temperature, near the plasma edge. For good coupling, the plasma in the immediate vicinity of the antenna must have a sufficiently low beta, $\beta << m_e/m_i$. We show that the most important parameter in this respect is the edge plasma density: when it is large, the electrons screen efficiently the component of the wave electric field parallel to the static magnetic field, which is essential for coupling to slow plasma waves. This suggests that protecting the antenna with lateral auxiliary limiters protruding somewhat into the scrape-off plasma might considerably improve coupling. The value of the edge density gradient on the other hand has no influence on the coupling within the range explored. An increase in the scrape-off ion temperature improves matching by increasing the BW wavelength. We also find that a quadrupole T-antenna with central feeder and shorts at the ends is better matched than a dipole one with feeders at the ends and short in the middle.

2 - The field in vacuum.

In vacuum we must distinguish three regions, as indicated in Fig. 1. For convenience, we will use throghout units of length such that $\omega/c = 1$. In each layer, the fields of each partial wave in Eq. (1) can be written as follows:

a) Between the plasma edge and the Faraday shield $(-s < x < 0)$:

$$\begin{aligned}
E_y =& E_y^b \cosh(\nu_x x) - i\nu_x B_z^b \sinh(\nu_x x) \\
B_z =& \left[- n_y n_z B_y^b + (1 - n_z^2) B_z^b \right] \cosh(\nu_x x) \\
&+ i\nu_x^{-1} \left[(1 - n_z^2) E_y^b + n_y n_z E_z^b \right] \sinh(\nu_x x) \\
E_z =& E_z^b \cosh(\nu_x x) + i\nu_x B_y^b \sinh(\nu_x x) \\
B_y =& \left[(1 - n_y^2) B_y^b - n_y n_z B_z^b \right] \cosh(\nu_x x) \\
&- i\nu_x^{-1} \left[n_y n_z E_y^b + (1 - n_y^2) E_z^b \right] \sinh(\nu_x x)
\end{aligned} \tag{3}$$

b) Between the Faraday shield and the antenna $(-a < x < -s)$:

$$\begin{aligned}
E_y =& E_y^a \cosh(\nu_x (x+a)) - i\nu_x B_z^a \sinh(\nu_x (x+a)) \\
B_z =& \left[-n_y n_z B_y^a + (1 - n_z^2) B_z^a \right] \cosh(\nu_x (x+a)) \\
&+ i\nu_x^{-1} \left[(1 - n_z^2) E_y^a + n_y n_z E_z^a \right] \sinh(\nu_x (x+a)) \\
E_z =& E_z^a \cosh(\nu_x (x+a)) + i\nu_x B_y^a \sinh(\nu_x (x+a)) \\
B_y =& \left[(1 - n_y^2) B_y^a - n_y n_z B_z^a \right] \cosh(\nu_x (x+a)) \\
&- i\nu_x^{-1} \left[n_y n_z E_y^a + (1 - n_y^2) E_z^a \right] \sinh(\nu_x (x+a))
\end{aligned} \tag{4}$$

c) Between the antenna and the plasma edge $(-w < x < -a)$

$$\begin{aligned}
E_y &= \frac{\sinh(\nu_x (w+x))}{\sinh(\nu_x (w-a))} E_y^a \\
B_z &= + \frac{i}{\nu_x} \frac{\cosh(\nu_x (w+x))}{\sinh(\nu_x (w-a))} \left[(1 - n_z^2) E_y^a + n_y n_z E_z^a \right] \\
E_z &= \frac{\sinh(\nu_x (w+x))}{\sinh(\nu_x (w-a))} E_z^a \\
B_y &= - \frac{i}{\nu_x} \frac{\cosh(\nu_x (w+x))}{\sinh(\nu_x (w-a))} \left[n_y n_z E_y^a + (1 - n_y^2) E_z^a \right]
\end{aligned} \tag{5}$$

In these equations $-\nu_x^2 = 1 - n_y^2 - n_z^2$, with the convention that if $\nu_x^2 < 0$, $\nu_x \rightarrow -i\sqrt{(} - n_x^2)$, so that trigonometric instead of hyperbolic functions would appear in these equations.

Although not making explicit reference to TE and TM modes, this representation of the vacuum field facilitates the task of imposing the appropriate matching conditions.

In writing Eqs. (3)-(5), we have already taken into account that both E_y and E_z are continuous at the antenna and vanish at the wall. We now list the other conditions which determine the eigth constants E_y^b to B_z^a.

a) Conditions at the antenna. Let the current in the antenna flow in the direction making an angle α with the vertical (poloidal) direction ($\alpha = 0$ for Fast Wave excitation, $\alpha = \pi/2$ for Bernstein Wave excitation). Let further

$$\begin{aligned} \vec{J} &= \sum_{n_y,n_z} \left\{ J^a(n_y,n_z) e^{i(n_y y + n_z z)} \right\} \cdot \vec{e}_\alpha \\ \vec{e}_\alpha &= (\cos\alpha \vec{e}_y - \sin\alpha \vec{e}_z) \end{aligned} \tag{6}$$

be the Fourier decomposition of the current distribution in the antenna plane $x = -a$; $\vec{e}_y$ and $\vec{e}_z$ are unit vectors in the y and z direction, respectively (the most common types of antennas and the Fourier transform of their current distributions are presented in Appendix C). The jump conditions for the magnetic field at this plane are:

$$\begin{aligned} -\frac{i}{\nu_x}\frac{\cosh(\nu_x(w-a))}{\sinh(\nu_x(w-a))}\left[(1-n_z^2)E_y^a + n_y n_z E_z^a\right] \\ +\left[(1-n_z^2)B_z^a - n_y n_z B_y^a\right] = \frac{4\pi}{c} J^a \cos\alpha \\ +\frac{i}{\nu_x}\frac{\cosh(\nu_x(w-a))}{\sinh(\nu_x(w-a))}\left[n_y n_z E_y^a + (1-n_y^2)E_z^a\right] \\ +\left[-n_y n_z B_z^a + (1-n_y^2)B_y^a\right] = \frac{4\pi}{c} J^a \sin\alpha \end{aligned} \tag{7}$$

b) Conditions at the Faraday Shield. The Faraday shield is usually modelled as a sheet with anysotropic conductivity, infinite in one direction, and zero in the orthogonal one. In most cases, the shield conductors are orthogonal to those of the antenna; we will however allow for an arbitrary orientation, making an angle β to the horizontal (toroidal) direction. The electric field component $\vec{E} \cdot \vec{e}_\beta$ must vanish on both sides of the shield:

$$\begin{aligned} \cosh(\nu_x s)[E_y^b \sin\beta + E_z^b \cos\beta] \\ +i\nu_x \sinh(\nu_x s)[B_y^b \cos\beta - B_z^b \sin\beta] = 0 \\ \cosh(\nu_x(a-s))[E_y^a \sin\beta + E_z^a \cos\beta] \\ -i\nu_x \sinh(\nu_x(a-s))[B_y^a \cos\beta - B_z^a \sin\beta] = 0 \end{aligned} \tag{8}$$

Further, we must require the continuity of the component of $\vec{E} \times \vec{e}_\beta$ in the shield plane:

$$\begin{aligned} \cosh(\nu_x s)[E_y^b \cos\beta - E_z^b \sin\beta] \\ +i\nu_x \sinh(\nu_x s)[B_y^b \sin\beta - B_z^b \cos\beta] = \\ = \cosh(\nu_x(a-s))[E_y^a \cos\beta - E_z^a \sin\beta] \\ -i\nu_x \sinh(\nu_x(a-s))[B_y^a \sin\beta + B_z^a \cos\beta] \end{aligned} \tag{9}$$

and of the component $\vec{B} \cdot \vec{e}_\beta$ of the wave magnetic field:

$$\begin{aligned} &\cosh(\nu_x s)[g_y B_y^b + g_z B_z^b] \\ &\qquad -i\nu_x^{-1} \sinh(\nu_x s)[-g_z E_y^b + g_y E_z^b] = \\ &= \cosh(\nu_x(a-s))[g_y B_y^a + g_z B_z^a] \\ &\qquad +i\nu_x^{-1} \sinh(\nu_x(a-s))[-g_z E_y^a + g_y E_z^a] \end{aligned} \tag{10}$$

where

$$\begin{aligned} g_y &= (1 - n_y^2)\sin\beta - n_y n_z \cos\beta \\ g_z &= -n_y n_z \sin\beta + (1 - n_z^2)\cos\beta \end{aligned} \tag{11}$$

This model for the Faraday shield is well justified in the case of FW antennas: E_z is anyhow very small also in the plasma, so that the presence of the additional constraint $E_z = 0$ at the screen amounts to eliminate E_z altogether. In the case of BW launching, on the contrary, plasma and Faraday shield screen orthogonal components of $\vec{E}$; if the latter extends over the whole plane $x = -s$, a kind of waveguide with anisotropic walls is created between this plane and the plasma surface. Excitation of guided modes in this layer, combined with the effective periodicity attributed to the system by the discrete Fourier expansion (1), gives rise to strong resonances in the coupling resistance of the antenna, which obviously do not exist in the real configuration. In this case it is therefore imperative to take into account that the Faraday screen exists only in front of the antenna.

To do this exactly is quite difficult, since it would require to give up the Fourier decomposition (1) of the field. Thus we have assumed the above description of the Faraday shield to be valid for modes with small n_y (for $n_y = 0$ obvously the presence of a single point at which $E_y = 0$ implies that E_y vanishes everywhere), while for large n_y we have neglected the presence of the screen altogether, assuming (3) to be valid up to the antenna plane $x = -a$. The radiation resistance is then a monotonically decreasing function of the distance between the antenna and the plasma, and does not depend on the precise value of n_y above which the screen is neglected, provided it is low enough to avoid the excitation of guided modes in vacuum. It should also be noted that guided modes disappear when the plasma is in direct contact with the shield, in which case the infinite and the localised shield give almost identical results.

c) Conditions at the plasma edge. The boundary conditions at the plasma edge are most easily written in terms of the surface impedance matrix of the plasma. This matrix expresses the linear relation between electric and magnetic field components at the plasma surface for the waves satisfying the appropriate outward radiation conditions

far from the antenna:

$$\begin{aligned} E_y(0) = E_y^b &= Z_{11}B_z(0) + Z_{12}B_y(0) \\ E_z(0) = E_z^b &= Z_{21}B_z(0) + Z_{22}B_y(0) \end{aligned} \tag{12}$$

(all quantities in this equation have to be understood as functions of n_y and n_z). If the matrix Z_{ij} is known, the continuity of the magnetic field can be imposed as a condition relating E_y^b and E_z^b to B_z^b and B_y^b:

$$\begin{aligned} E_y^b &= \left[(1-n_z^2)Z_{11} - n_y n_z Z_{12}\right] B_z^b + \left[-n_y n_z Z_{11} + (1-n_y^2)Z_{12}\right] B_y^b \\ E_z^b &= \left[(1-n_z^2)Z_{21} - n_y n_z Z_{22}\right] B_z^b + \left[-n_y n_z Z_{21} + (1-n_y^2)Z_{22}\right] B_y^b \end{aligned} \tag{13}$$

Eqs. (7) to (13) completely determine the unknown coefficients in Eqs. (3) to (5) in terms of the antenna current spectral decomposition, $J^a(n_y, n_z)$, the angles α and β, and the surface impedence matrix of the plasma, Z_{ij}. In spite of its complicated appearence, this system can be easily solved analytically, as sketched in Appendix A. The explicit solution is useful to gain insight into the mechanism of wave launching, and advantageous over numerical inversion. Moreover, its availability makes it possible in principle to determine the current distribution in the antenna selfconsistently by the variational approach of Teilhaber and Jacquinot [22].

3 - Propagation in the Plasma.

a) The wave equations. The next step is the evaluation of the surface impedance matrix (12). The set of equations to be solved in the plasma can be deduced from the work of Swanson [25], Colestock and Kashuba [26], and Brambilla and Ottaviani [27]. For each partial plane wave they are:

$$\begin{aligned} -\left(\frac{d}{dx} + n_y\right)\left[\sigma\left(\frac{d}{dx} - n_y\right)(E_x + iE_y)\right] + (n_y^2 + n_z^2 - S)E_x \\ + in_y\frac{dE_y}{dx} + iDE_y - in_z\frac{dE_z}{dx} = 0 \\ i\left(\frac{d}{dx} + n_y\right)\left[\sigma\left(\frac{d}{dx} - n_y\right)(E_x + iE_y)\right] + in_y\frac{dE_x}{dx} - iDE_x \\ -\frac{d^2E_y}{d^2x} + (n_z^2 - S)E_y - n_y n_z E_z = 0 \\ in_z\frac{dE_x}{dx} - n_y n_z E_y - \frac{d^2E_z}{d^2x} + (n_y^2 - P)E_z = 0 \end{aligned} \tag{14}$$

Introducing Stix notations [28] for the Zero Larmor radius limit of the dielectric tensor elements, and approximations approriate to the ion cyclotron frequency range,

$$
\begin{aligned}
L &= 1 + \frac{\omega_{pe}^2}{\Omega_{ce}^2}\left(1 - \frac{\Omega_{ce}}{\omega}\left(1 - i\frac{\nu_e}{\omega}\right)\right) - \sum_i \frac{\omega_{pi}^2}{\Omega_{ci}^2} x_{oi} Z(x_{1i}) \\
R &= 1 + \frac{\omega_{pe}^2}{\Omega_{ce}^2}\left(1 + \frac{\Omega_{ce}}{\omega}\left(1 - i\frac{\nu_e}{\omega}\right)\right) - \sum_i \frac{\omega_{pi}^2}{\Omega_{ci}^2} \frac{\omega}{\omega + \Omega_{ci}} \\
P &= 1 - \frac{\omega_{pe}^2}{\omega^2}\left(1 - 2i\frac{\nu_e}{\omega}\right) x_{oe}^2 Z'(x_{oe}) \\
S &= \frac{R+L}{2} \qquad\qquad D = \frac{R-L}{2}
\end{aligned}
\tag{15}
$$

Among FLR corrections, it is justified to retain only the one which is resonant near the first harmonic of the ion cyclotron frequency (for a discussion, cfr. [29]):

$$
\sigma = \frac{1}{4} \sum_i \frac{\omega_{pi}^2}{\Omega_{ci}^2} \frac{v_{thi}^2}{c^2} \left(-x_{oi} Z(x_{2i})\right) \tag{16}
$$

Here

$$
Z(x) = \frac{1}{\sqrt{\pi}} \int_{-\infty}^{\infty} \frac{e^{-u^2}}{u - x} du + i\sqrt{\pi} e^{-x^2} \tag{17}
$$

is the Plasma Dispersion Function [30], with

$$
x_{n,i} = \frac{\omega - n\Omega_{ci}}{k_z v_{thi}} \tag{18}
$$

Finally ν_e is the electron collision frequency; we have used the correct form for collisional damping in the cold plasma limit, which is adequate as long as $|x_{o,e}| >> 1$, a condition always satisfied near the plasma edge where collisional damping is most important.

To these equations we may add the definitions of the magnetic field components in the plasma, which follow from Maxwells equation $\vec{\nabla} \times \vec{E} = i\frac{\omega}{c}\vec{B}$, and are needed to impose the boundary conditions at the plasma edge:

$$
B_x = n_y E_z - n_z E_y; \qquad B_y = n_z E_x + i\frac{dE_z}{dx}; \qquad B_z = -i\frac{dE_y}{dx} - n_y E_x \tag{19}
$$

In the particular case $n_y = 0$ Eqs. (14) are similar, but not identical, with those solved in Ref. [17]. The difference is in the form of the FLR corrections, which are here in a form which is, as it should, selfadjoint when the dielectric tensor is Hermitean, i.e. the plasma is dissipationless. This form has been obtained in Refs. [25] - [26] by integrating Vlasov equation in the same geometry as the one used here.

The power balance equation associated with Eqs. (14) is:

$$\frac{dP_x}{dx} = -W_a \tag{20}$$

where the power flux P_x and the power dissipated per unit volume W_a are respectively:

$$P_x = \frac{c}{8\pi}\left\{ Re\left(E_y^* B_z - E_z^* B_y\right) + Im\left[(E_x + iE_y)^*\left[\sigma\left(\frac{d}{dx} - n_y\right)(E_x + iE_y)\right]\right]\right\} \tag{21a}$$

and

$$W_a = \frac{c}{8\pi}\left\{ -Im(\sigma)\left|\left(\frac{d}{dx} - n_y\right)(E_x + iE_y)\right|^2 + Im(L)|E_x + iE_y|^2 + \right.$$
$$\left. + Im(P)|E_z|^2 \right\} \tag{21b}$$

The last term in P_x is the kinetic contribution of the power flux, which in the case of BW excitation is usually larger than the electromagnetic part. In W_a we recognise successively first harmonic ion cyclotron damping (HICD), ion cyclotron damping at the fundamental (ICD), and electron Landau damping (ELD). Magnetic Pumping of the electrons has been neglected, since it is normally very small in the outer layers of the plasma, but the relevant terms could be easily added to Eqs. (14) and (21).

b) The WKB limit. To understand the physics beyond these equations, and to impose the appropriate radiation conditions to the solution, it is useful to discuss briefly the dispersion relation which is obtained where the WKB approximation can be applied ($d/dx \rightarrow in_x$; $n_\perp^2 = n_x^2 + n_y^2$):

$$(n_\perp^2 - P)\left\{-\sigma n_\perp^4 + [(n_z^2 - S)n_\perp^2 + 2\sigma(n_z^2 - R) + (n_z^2 - R)(n_z^2 - L)]\right\}$$
$$-n_z^2 n_\perp^2[(1+\sigma)n_\perp^2 + (n_z^2 - S)] \tag{22}$$

The three roots of this equation can with good accuracy be approximated as

$$n_\perp^2 \cong n_\perp^2)_F = -\frac{(n_z^2 - R)(n_z^2 - L)}{(n_z^2 - S)}$$
$$n_\perp^2 \cong n_\perp^2)_S = -(n_z^2 - S)\frac{P}{S} \tag{23}$$
$$n_\perp^2 \cong n_\perp^2)_B = -\frac{(n_z^2 - S)}{\sigma}$$

The subscripts stay for fast, or compressional wave, slow or torsional wave, and Bernstein wave, respectively. The slow wave is strongly evanescent if $|x_{oe}| = |\omega/(k_\parallel v_{the})| >> 1$, but goes over into a short wavelength propagating wave, known as Kinetic Alfven wave, in the opposite limit, $|x_{oe}| << 1$. The Bernstein wave propagates at frequencies below the first harmonic of the IC frequency, and is evanescent above. As well known,

the above factorisation fails only in the vicinity of the layer $\omega = 2\Omega_{ci}$, where the Bernstein wave has a confluence with the fast wave (Cfr. Weynants, [31], or the discussion in [29]), and near ion-ion resonances. At frequencies larger than the majority ion cyclotron frequency, moreover, it can fails at the Lower Hybrid resonance near the Faraday screen if the density decreases sufficiently rapidly in the scrape off plasma [23].

For our purposes it is important to realize that, in all cases, only two of the three WKB solutions (23) are simultaneously acceptable. The largest root always corresponds to a wavelength shorter than one ion Larmor radius, and therefore violates the assumption $k_\perp \rho_i << 1$, under which Eqs (14) and (22) have been obtained. An investigation of the complete hot plasma dispersion relation shows that in the vast majority of cases it has only two solutions, both satisfying the conditions for FLR expansion; when a third root exists for which this is not true (e. g. the backward Bernstein wave near higher cyclotron harmonics), it has nothing to do with the spurious root of Eqs. (22).

Which root has to be discarded depends on the plasma pressure: it is not difficult to show ([29], [31]) that the physically relevant wave is the slow cold plasma wave if $\beta << m_e/m_i$, and the Bernstein wave as soon as β approaches or exceeds m_e/m_i. As stressed e.g by Ono [14], there is a continuous transition from one wave into the other as the plasma pressure increases. It is therefore impossible to find a meaningful approximation to the system (14) which eliminates the spurious wave by reducing its order by two, yet is valid uniformly for plasma all pressures. The usual solution to this problem is to take the limit $m_e/m_i \to 0$, or $|P| \to \infty$, thereby eliminating the slow cold plasma wave altogether, on the ground that the condition $\beta \gtrsim m_e/m_i$ is usually well satisfied in a tokamak, even relatively close to the plasma edge. The zero electron inertia limit is well justified when investigating coupling and propagation of the compressional wave, but is inadequate in the present case. More precisely, when the plasma is so dense that this approximation is justified down to its boundary, no appreciable coupling through external currents flowing in the direction of the static magnetic field is possible. The reason is that under this conditions the plasma is for all purposes a perfect conductor along the field lines, so that image currents on the plasma surface will completely screen out any external B_y (the parallel component of the wave field, E_z, does not vanish when FLR effects are taken into account, but is then completely determined by the values of the perpendicular components). Under these conditions, only the compressional wave can be excited. Thus to make launching of Bernstein waves possible, a low density plasma layer must exist near the antenna. In turn, to describe this situation, the full system (14) has to be retained, and the spurious solution must be eliminated by imposing the appropriate boundary conditions.

c) Radiation and edge boundary conditions. To exclude explicitly the cold plasma wave at the high density point we write the outward radiation conditions in the form

$$\begin{aligned} \vec{E} &= \tau_F \vec{E}_F + \tau_B \vec{E}_B \\ \frac{d\vec{E}}{dx} &= i n_{xF} \tau_F \vec{E}_F + i n_{xB} \tau_B \vec{E}_B \end{aligned} \tag{24}$$

The sign to be attributed to n_{xF}, n_{xB}, and the ratio of the field components in the amplitudes E_F and E_B of the Fast and Bernstein wave, respectively, are easily determined by examining the WKB limit of Eqs. (15) and (23) with $m_e/m_i << 1$:

$$\begin{aligned} \frac{E_x}{E_y} &= \frac{n_x n_y - i(D + \sigma n_\perp^2)}{\sigma n_\perp^2 + n_y^2 + n_z^2 - S} \\ \frac{E_z}{E_y} &= \frac{n_z}{n_\perp^2 - P}\left(n_x \frac{E_x}{E_y} + n_y\right) \end{aligned} \tag{25}$$

The system (14) must then be integrated backwards toward the plasma edge, with a sufficient accuracy to ensure that the solution will remember conditions (25) throughout. The unknown transmission amplitudes τ_F and τ_B must be finally determined from the conditions at the plasma-vacuum interface $x = 0$.

To evaluate the surface impedance matrix Z_{ij} as required by the formulation of the previous section, Eqs. (14) have to be solved twice, imposing successively

$$a) \quad (B_y(0) = 1, B_z(0) = 0)\,; \qquad b) \quad (B_y(0) = 0, B_z(0) = 1) \tag{26}$$

Using Eqs. (19), these conditions are immediately translated into boundary conditions appropriate to the system (14). The values of the electric field at $x = 0$ are then directly the elements of Z_{ij}.

Because the system (14) is formally of sixth order, however, the boundary conditions (24) and (26) are still not sufficient to determine the solution uniquely. The additional condition to be imposed is easily determined by integrating Eqs. (14) over an infinitesimal interval across the plasma-vacuum boundary. In addition to the continuity of E_y, E_z, B_y, B_z, it is found in this way that the condition

$$\sigma(0)\Big\{\Big(\frac{dE_x(0)}{dx} + i\frac{dE_y(0)}{dx}\Big) - n_y\big(E_x(0) + iE_y(0)\big)\Big\} = 0 \tag{27}$$

must be explicitly imposed upon the solution whenever $\sigma(0)$ does not vanish. Inspection of Eq. (21) shows that this condition makes the kinetic part of the power flux vanish at the plasma boundary, and thereby ensures the continuity ot the total flux there, in spite of the discontinuity of the wave equations coefficients.

It would be clearly hopeless to attempt the solution of Eqs. (14) with the boundary conditions (24) - (27) using a Runge-Kutta method. Instead, we have used a Finite Element (FE) discretisation with cubic Hermite interpolating functions, which is ideally suited to this problem. As shown in Appendix C, the FE discretization, if properly formulated, automatically tries to satisfy the energy balance equation (20) as accurately as possible; this in turn minimizes pollution by solutions not allowed by the boundary conditions. Thus for example numerical instabilities due to unwanted exponential solutions never arise. Moreover, accuracy can be efficiently achieved by adapting the mesh locally to the shorter wavelength which needs to be resolved: for this purpose, a superficial examination of the dispersion relation is sufficient, even where the WKB approximation is obviously non valid. By taking 5 to 10 mesh points per wavelength (somewhat more near the plasma edge), a relative accuracy of 10^{-6} is easily obtained. Finally, all the boundary conditions arising in the present problem are of the so-called natural type (involving explicitly a first derivative), which are most easily enforced within the FE formalism.

4. - Coupling to Bernstein waves.

As an application of our code we have tried to simulate coupling of Bernstein waves in the Alcator C tokamak [13]. The parameters of the plasma and of the antenna are listed in Table 1. For the simulation, the asymptotic radiation conditions where imposed 4.5 cm inside the limiter edge: this is certainly enough for the Bernstein wave, but possibly not for the fast one. To make sure that this does not influence the results, we have run a few cases assuming a high standing wave ratio for the fast wave. For the purpose, Eqs. (24) was replaced by

$$\begin{aligned} \vec{E} &= \tau_F \left(1+\rho\right) \vec{E}_F + \tau_B \vec{E}_B \\ \frac{d\vec{E}}{dx} &= i n_{xF} \tau_F \left(1-\rho\right) \vec{E}_F + i n_{xB} \tau_B \vec{E}_B \end{aligned} \tag{28}$$

where $|\rho|$ was taken close or equal to unity, and the phase of ρ was estimated with a simple WKB model. The radiation resistance of the antenna was little affected (less than 10%), and the part due to BW not at all.

a) Variations with magnetic field intensity. The Alcator experiment were performed at a fixed frequency (183.6 Mhz), varying the intensity of the static magnetic field. The set of parameters used in our code for a similar a magnetic field scan are listed in Table 1. We have supposed throughout that the scrape-off plasma extends out to the Faraday shield. For a scrape-off width of 0.5 cm and a density decay length of 0.25 cm from the limiter value of $0.60 \cdot 10^{13}$ cm^{-3}, this means a density of $8.12 \cdot 10^{11}$ cm^{-3} at the screen. Fig. 3 is a plot of the radiation resistance of the antenna versus the ratio ω/Ω_{ci} at the limiter radius $r = a$ under these assumptions. For the frequency chosen, the first harmonic resonance of Hydrogen is located at $r = a$ when $B(0) = 6.845$ Tesla. At fields lower than this value the radiation resistance is quite small ($\lesssim 0.05$ Ohms): this is to be expected, since Bernstein waves are evanescent, and the antenna has the wrong orientation to launch the fast wave efficiently. The radiation resistance raises to a peak of somewhat less than 1.3 Ohms at the value of the magnetic field which puts the resonance just behind the antenna, and decreases slowly again as the field increases further. The slow decrease at higher magnetic fields can be explained by the decrease in the wavelength of the Bernstein waves, which makes matching increasingly difficult. The value of the radiation resistance when the first harmonic resonance is just behind the antenna is close to the measured one; this is also the range in which efficient heating was observed. Outside this range, however, the calculated value is almost an order of magnitude smaller than the observed one. Even multiplying the Coulomb collision frequency by a factor 10 increases the computed R_a by 10 to 20% only. Other parasitic absorption mechanisms, or nonlinear effects [33] might be responsible for the discrepancy.

Fig. 4 shows the fraction of power coupled to Bernstein waves, and the fraction absorbed by electrons and ions in the near field region (i.e. integrated from the antenna to the point at which the radiation conditions are imposed; this point is of course to some extent arbitrary). To the left of the resonance, practically all the power is found in the fast wave, as expected. Optimum coupling to the Bernstein waves occurs just above the resonance peak in the ion absorption. For still higher magnetic fields the fraction of power launched in the fast mode increases again, and is close to 30% at $\omega/\Omega_{ci} = 1.9$. Electron absorption is almost absent at low magnetic fields, and accounts for about 15% of the power when Bernstein waves are present. It should be noted that electron Landau damping is a strongly increasing function of density and temperature; therefore more of it is found if the asymptotic point is displaced towards the plasma interior, at the expense of the power in the Bernstein waves. In addition, the power deposited in the electrons includes about 5% collisional damping localised mainly very close to the plasma boundary.

It is perhaps more appropriate to compare the different power channels at a constant value of the current in the antenna; this is done in Fig. 5. The existence of an optimum magnetic field for Bernstein waves launching is made even more obvious by this representation of the results. The amount of electron heating is closely proportional to the power in the Bernstein waves; the power coupled to the Fast wave, on the other hand, is roughly constant over the whole range explored, except for a dip corresponding to the domain where ion damping is strong and partial waves with small n_z are evanescent in the immediate vicinity of the antenna ([31],[32]).

It is also interesting to investigate the spectral distribution of the power among the partial waves in the superposition (1). From the physical point of view, the most informative is the n_z spectrum (summed over n_y), shown in Fig. 6a, 7a and 8a for the cases $\omega/\Omega_{ci} = 2.02$, 1.99 and 1.96 at $r = a$, respectively. The overall shape of the spectrum is almost frequency independent; the distribution of the power among the various channels is however different in the three cases, as one would expect from elementary considerations.

It is interesting to remark that for an antenna oriented along the static magnetic field the width of the n_z spectra corresponds roughly to that of the Fourier spectrum of the antenna current itself. This is due to the fact that Bernstein waves are propagative from the very edge of the plasma; in this respect they differ drastically from the Fast wave, which is evanescent up to the R cut-off, a feature which strongly suppresses waves with large $|n_z|$ from the radiated spectrum.

The Alcator antenna has a central feeder and shorts at the ends, so that the current distribution is of the quadrupole type, and has an antisymmetric n_z spectrum. This is however not the only cause of the deep minimum in the spectra near $n_z = 0$: Bernstein waves with $n_z = 0$ cannot be directly coupled from outside, since they have E_z identically zero, as easily seen from Eqs. (14). As a consequence, the n_z spectrum launched by a dipole antenna (feeders at the extremes and central short, current in the same direction in the whole conductor), but otherwise of the same dimensions and for the same plasma parameters as in Figs. 9a, is also depleted near $n_z = 0$, as shown in Fig. 9. The poor coupling of low n_z modes has the consequence that the dipole antenna has a radiation resistance of only 0.15 Ohms, less than one third of that of the quadrupole antenna under the same conditions. In other words, although accessibility in the sense which applies to the coupling of Lower Hybrid waves [34] plays no role here, the rough proportionality of Ez to n_z imposes similar requirements on the antenna design for efficient coupling.

The n_y spectra for given n_z, on the contrary, are sharply limited towards larges $|n_y|$ by the decrease of the surface admittance of the plasma, and are therefore much narrower than the corresponding Fourier spectrum of the antenna current. This implies that the poloidal distribution of the field in the plasma will be relatively broad, in spite of the very thin antenna used.

Figs. 6b, 7b and 8b show the absorption per unit volume as a function of radial position (averaged over the whole magnetic surface, and for one MW coupled power). As already mentioned, ELD is negligible near the plasma edge, and increases towards the plasma interior when Bernstein waves are excited. Collisional damping is in all cases sharply localised near the plasma boundary, essentially where the h.f. electric field component parallel to the static magnetic field is also large. This means that collisions are much more efficient in dissipating the parallel electron motion than their $\vec{E} \times \vec{B}$ drift. HICD on the other hand is localised around the second harmonic. If only the fast wave is launched (fig. 6b), HICD is much weaker than when Bernstein waves are also excited (fig. 7b), since its efficiency is proportional to $k_\perp^2 \rho_i^2$.

Finally, Figs. 6 to 8 c and d show the the components E_x and E_z of the electric field, along a radius starting from the antenna at 2/3 of its half length from the centre (the reason to choose this position rather than the center of the antenna is that E_z vanishes there in the quadrupole case, E_x in the dipole case). The numerical values in these figures (in kV/cm) correspond to the fields required to launch one MW into the plasma; the two curves are the real and imaginary part, respectively. The difference between situations with propagating and evanescent Bernstein waves is clearly seen.

Beyond the first one or two centimeters from the plasma edge the parallel component E_z agrees extremely well with the second of Eqs. (25), with $n_\perp$ estimated from the logarithmic derivative of the solution. One can roughly locate the wave transformation from the shear cold plasma wave to the Bernstein wave at the point where Eqs. (25) begin to be accurate. The values of E_x and E_z fields associated with the cold plasma wave are clearly much larger than those associated with the Bernstein wave for the same trasmitted power flux.

b) Dependency on the plasma edge parameters. To investigate how coupling depends on the conditions in the boundary layer, we have kept the magnetic field at the value $B_o = 6.98$ Tesla ($\omega = 1.96\Omega_{ci}$ at the edge) and we have first varied the distance of the antenna from the limiter assuming that the density and temperature at $r = a$ and their e-folding lengths remain constant. Under this assumption, both n_e and $T_{e,i}$ decrease at the Faraday shield radius. Fig. 10 shows that the radiation resistance increases rapidly

as the boundary density decreases. This illustrates again the essential role of the parallel component of the electric field in coupling to Bernstein waves. The amplitude of E_z in the plasma for a given antenna current is roughly inversely proportional to the density; in the limit of very large edge density the antenna sees an almost perfectly conducting surface and cannot radiate.

To show that the important parameter is the edge density rather than for example the density gradient, we have run a series in which the width of the scrape-off plasma was kept constant, but the e-folding lengths of both n_e and $T_{e,i}$ where varied instead, so as to have the same values at the Faraday shield as in the previous series, but with sharper and sharper gradients. When plotted on the same scale (Fig. 11), this series is almost identical to the previous one. Finally, Fig. 12 shows a series in which the scrape-off width and the e-folding lengths were varied simultaneously so as to keep n_e and $T_{e,i}$ constant in front of the shield: in this case the radiation resistance is almost constant.

No experiment in which the scrape-off plasma parameters were varied in a controlled way is available for comparison with these code predictions. In addition, the density and temperature in the scrape-off layer could be influenced by the HF power itself, and be different from those measured when the HF is turned off. It is therefore risky to attempt to anticipate how coupling would evolve when the plasma moves away from the antenna during the heating pulse, as it happens at the transition from L to H regimes. Nevertheless it is tempting to suggest that a BW antenna could tolerate this transition much better than conventional FW antennas ([35]). Also, an effort to keep the plasma density in contact with the Faraday screen as low as possible, for example using lateral protections protruding somewhat into the scrape-off layer, might well pay in terms of antenna loading.

Increasing the ion temperature in the scrape-off plasma also favors coupling, as seen from Fig. 13. The reason for this is the fact that the wavelength of the slow waves increases with T_i, thereby facilitating matching.

Conclusions. The coupling resistance of an antenna designed to launch Bernstein waves is found to be very sensitive to the details of the density profile near the Faraday screen. For good matching, a low density layer should exist near the plasma edge. A quite clear-cut prediction of this theory is that coupling will be very poor if the discharge moves towards the antenna so that a high density plasma comes in direct contact with the Faraday screen. This might explain the high density cut-off observed

in some experiments, although other effects, such as large edge density fluctuations, probably also play a role [13].

Under conditions for optimum matching, comfortably large values of the radiation resistance can be achieved, comparable or even larger than those typical for Fast Wave launching. To help achieving these conditions relatively independently from the plasma dendity, lateral protection of the antenna could be useful. We have also shown that a quadrupole antenna (central feeder, shorts at the ends, antisymmetric current distribution) is appreciably better matched than a dipole antenna (feeders at the end, central short, symmetric current distribution).

Appendix A - The transmission line model for the antenna current.

In principle, the current distribution $\vec{J}_a(y,z)$ in the antenna is one of the unknowns of the problem. In most cases however, a plausible assumption can be made about $\vec{J}_a$, thereby circumventing a lengthy selfconsistent evaluation. For antennas with thin and long elements, each conductor can be approximately treated as a segment of transmission line, with appropriate boundary conditions to be applied at feeders and shorts. This approach has been widely used in the literature; moreover, the selfconsistent solution of Tailhaber and Jacquinot [22] also uses a transmission line representation of the antenna current distribution, in which however the characteristics of the line are evaluated via a variational principle, and harmonics of the basic line propagation wavenumber are admitted.

In this Appendix we sketch the transmission line model in its simplest form, and we give a few examples of the most common experimental set-ups. The goal is in each case to compute the Fourier transform of the antenna current with respect to the two directions y and z to be used in Eq. (1).

a) Periodicity form factor along the torus. Let us first of all assume that N_a identical antennas are symmetrically disposed around the torus, and that adiacent ones are excited with a phase difference ψ_a. It is immediately seen that this has the effect of introducing in the Fourier spectrum $J_a(n_y,n_z)$ an additional factor (length are measured in units of c/ω):

$$F_a(n_z) = \frac{\sin\frac{N_a}{2}\left(\psi_a + \frac{2\pi}{N_a}\frac{n_z}{R_T}\right)}{\sin\frac{1}{2}\left(\psi_a + \frac{2\pi}{N_a}\frac{n_z}{R_T}\right)} \qquad (A1)$$

Since $n_\phi = n_z R_T$ is an integer, when ψ_a is zero or π this factor amounts to a set of selection rules. On the other hand the individual spectrum of each antenna is usually so broad that this factor has no other appreciable influence on the global spectrum. In the ion cyclotron frequency range spectrum shaping has to be implemented by dephasing closely spaced conductors belonging to one and the same antenna; different antennas distributed around the tokamak are only weakly coupled to each other.

b) Orientation of the antenna. We want to consider antennas whose conductor are arbitrarily oriented with respect to the static magnetic field. For this purpose, with reference to Fig. 2, it is convenient to introduce coordinates η and ς in the plane of the antenna such that η is along the antenna conductors ($\vec{J}_a = \vec{e}_\eta J_a$). We also assume that

in the η, ς plane the current is factorised, so that

$$J(\eta,\varsigma) = \sum_{n_\eta, n_\varsigma} J_{(\eta)}(n_\eta) J_{(\varsigma)}(n_\varsigma) e^{i(n_\eta \eta + n_\varsigma \varsigma)} \qquad (A2)$$

(suffixes within parentesis do not mean vector components). Since

$$\eta = y\cos\alpha - \varsigma\sin\alpha \qquad \varsigma = y\sin\alpha + \varsigma\cos\alpha \qquad (A3)$$

it is immediately clear that

$$J(y,z) = \sum_{n_y, n_z} J_{(\eta)}(n_y\cos\alpha - n_z\sin\alpha) J_{(\varsigma)}(n_y\sin\alpha + n_z\cos\alpha) e^{i(n_y y + n_z z)} \qquad (A4)$$

It is thus sufficient to work out the two factors $J_{(\eta)}(n_\eta)$ and $J_{(\varsigma)}(n_\varsigma)$, where

$$n_\eta = n_y\cos\alpha - n_z\sin\alpha \qquad n_\varsigma = n_y\sin\alpha + n_z\cos\alpha \qquad (A5)$$

c) Spectrum in the direction perpendicular to the conductors. Assuming the current to be uniformly distributed in the cross-section of each conductor, the Fourier transform $J_{(\varsigma)}(n_\varsigma)$ is trivial. In the case of a dipole antenna with a single conductor of width w one has:

$$J_{(\varsigma)}(n_\varsigma) = \frac{2R_T}{\pi w} \frac{sin(n_\varsigma w/2)}{(n_\varsigma w/2)} \qquad (A6)$$

In the case of a quadrupole antenna with two parallel conductors excited with a phase difference ψ, one has:

$$J_{(\varsigma)}(n_\varsigma) = \frac{4R_T}{\pi w} \cos\left(\frac{n_\varsigma(g+w) - \psi)}{2}\right) \frac{sin(n_\varsigma w/2)}{(n_\varsigma w/2)} \qquad (A7)$$

If w is relatively large, the current generally has a tendency to peak towards the edges; this can be easily taken into account [19] but has usually little influence on the results.

d) Spectrum in the direction parallel to the conductors. The transmission line equation for each conductor are:

$$\frac{dE_x}{d\eta} = -\hat{z} J_\eta \qquad \frac{dJ_\eta}{d\eta} = -\hat{y} E_x \qquad (A8)$$

with

$$\hat{z} = R - i\omega L \qquad \hat{y} = -i\omega C \qquad (A9)$$

(here R,L,C are the resistance, inductance and capacitance per unit length). Hence in each homogeneous section of conductor we can write

$$E_x = E_o \cos \kappa(\eta - \eta_o) \qquad J_\eta = -\frac{E_o}{Z_a} \sin \kappa(\eta - \eta_o) \tag{A10}$$

whith

$$\kappa \simeq \omega\sqrt{LC}\left(1 + i\frac{R}{2\omega L}\right) \qquad Z_a \simeq \sqrt{\frac{L}{C}}\left(1 + i\frac{R}{2\omega L}\right) \tag{A11}$$

(generally R is so small that it is neglected altogether). The constants E_o and η_o have to be determined from the conditions at the feeders and at the shorts. We will now give two examples.

Central feeder, shorts at the ends. In this case, denoting with h the half-length of the conductor, we must impose:

$$E_x(0) = E_o \qquad E_x(\pm h) = 0 \tag{A12}$$

Hence

$$E_x = E_o \frac{\sin \kappa(h - |\eta|)}{\sin \kappa h} \tag{A13}$$

$$J_\eta = J_o \text{sign}(\eta) \frac{\cos \kappa(h - |\eta|)}{\cos \kappa h} \tag{A14}$$

where $J_o = -(E_o/Z_a) \cot \kappa h$. From the latter it is immediate to obtain:

$$J_{(\eta)}(n_\eta) = -\frac{i}{\pi} J_o \frac{n_\eta}{n_\eta^2 - \kappa^2} (\cos n_\eta h - \cos \kappa h) \tag{A15}$$

Central short, feeders at the ends in push-pull. In this case the boundary conditions are:

$$E_x(\pm h) = \mp E_o \qquad E_x(0) = 0 \tag{A16}$$

Hence

$$E_x = E_o \frac{\sin \kappa\eta}{\sin \kappa h} \qquad J_{(\eta)} = J_o \frac{\cos \kappa\eta}{\cos \kappa h} \tag{A17}$$

where again $J_o = -(E_o/Z_a) \cot \kappa h$. It is then immediate to obtain:

$$J_{(\eta)}(n_\eta) = \frac{h}{\pi} J_o \left\{ \frac{\sin (n_\eta - \kappa)h}{(n_\eta - \kappa)h} + \frac{\sin (n_\eta + \kappa)h}{(n_\eta + \kappa)h} \right\} \tag{A18}$$

More complicated cases can be similarly treated.

Appendix B - Solution for the field in vacuum.

We sketch here the analytic solution of Eqs. (7) to (12) for the vacuum fields, assuming that the surface impedance matrix Z_{ij} is known.

a) With Faraday shield. Beginning at the Faraday shield, the first three conditions there are satisfied if

$$\begin{aligned} E_y^b + i\nu_x^2 \hat{T}(s) B_z^b &= E_s \cos\beta \\ E_z^b - i\nu_x^2 \hat{T}(s) B_y^b &= -E_s \sin\beta \\ E_y^a - i\nu_x^2 \hat{T}((a-s)) B_z^a &= +\frac{\cosh(\nu_x s)}{\cosh(\nu_x(a-s))} E_s \cos\beta \\ E_z^a + i\nu_x^2 \hat{T}((a-s)) B_y^a &= -\frac{\cosh(\nu_x s)}{\cosh(\nu_x(a-s))} E_s \sin\beta \end{aligned} \tag{B1}$$

where E_s is an auxiliary unknown related to the electric field at $x = -s$, and $\hat{T}(x) = \sinh(\nu_x x)/(\nu_x \cosh(\nu_x x))$. It is convenient to regard these equations as defining E_y^b, E_z^b, E_y^a, E_z^a; they can be used to rewrite Eq. (9) for the parallel magnetic field component at the Faraday shield as:

$$\begin{aligned} \frac{1}{\cosh(\nu_x s)} \left(g_z B_z^b + g_y B_y^b\right) - \frac{1}{\cosh(\nu_x(a-s))} \left(g_z B_z^a + g_y B_y^a\right) = \\ = i \frac{\sinh(\nu_x a)}{\nu_x \cosh(\nu_x(a-s))} \nu_\beta^2 E_s \end{aligned} \tag{B2}$$

whith $\nu_\beta^2 = 1 - (n_y \sin\beta + n_z \cos\beta)^2$.

Turning next to the plasma edge, we use (B1) into (12) to obtain $B_z(0)$ and $B_y(0)$ in terms of E_s:

$$\begin{aligned} B_z(0) &= +\frac{E_s}{\Delta_s} \left(Z_{12}^s \sin\beta + Z_{22}^s \cos\beta\right) \\ B_y(0) &= -\frac{E_s}{\Delta_s} \left(Z_{11}^s \sin\beta + Z_{21}^s \cos\beta\right) \end{aligned} \tag{B3}$$

where

$$\begin{aligned} Z_{11}^s &= Z_{11} + i(1-n_y^2)\hat{T}(s) & Z_{12}^s &= Z_{12} + i n_y n_z \hat{T}(s) \\ Z_{21}^s &= Z_{21} - i n_y n_z \hat{T}(s) & Z_{22}^s &= Z_{22} - i(1-n_z^2)\hat{T}(s) \end{aligned} \tag{B5}$$

and

$$\Delta_s = Z_{11}^s Z_{22}^s - Z_{12}^s Z_{21}^s \tag{B6}$$

In particular therefore

$$g_z B_z^b + g_y B_y^b \equiv B_z(0)\cos\beta + B_y(0)\sin\beta = \Gamma_s E_s \tag{B6}$$

with

$$\Gamma_s = -\frac{1}{\Delta_s}\left[Z^s_{11}\sin^2\beta - (Z^s_{12} - Z^s_{21})\cos\beta\sin\beta - Z^s_{22}\cos^2\beta\right] \qquad (B7)$$

At the antenna, using (B1) again, the magnetic field on the plasma side can be written:

$$B_z(a_p) = (1-n_z^2)B_z^a - n_y n_z B_y^a \qquad B_y(a_w) = -n_y n_z B_z^a + (1-n_y^2)B_y^a \qquad (B8)$$

while on the wall side it is given by:

$$\begin{aligned} B_z(a_w) &= +i\nu_x^{-2}\hat{T}(w-a)\left[(1-n_z^2)E_y^a + n_y n_z E_z^a\right] = -\frac{\hat{T}(a-s)}{\hat{T}(w-a)}B_z(a) \\ &\quad - i\nu_x^{-2}\hat{T}(w-a)\frac{\cosh(\nu_x s)}{\cosh(\nu_x(a-s))}g_y \\ B_y(a_w) &= -i\nu_x^{-2}\hat{T}(w-a)\left[n_y n_z E_y^a + (1-n_y^2)E_z^a\right] = -\frac{\hat{T}(a-s)}{\hat{T}(w-a)}B_y(a) \\ &= +i\nu_x^{-2}\hat{T}(w-a)\frac{\cosh(\nu_x s)}{\cosh(\nu_x(a-s))}g_z \end{aligned} \qquad (B9)$$

Taking the appropriate linear combination gives:

$$\begin{aligned} g_z B_z^a + g_y B_y^a \equiv B_z(a_p)\cos\beta + B_y(a+)\sin\beta = \\ = \frac{\sinh(\nu_x(w-a))}{\sinh(\nu_x(w-s))}\left\{J^a\cosh(\nu_x(a-s))\cos(\alpha-\beta) + i\frac{\nu_\beta^2}{\nu_x^2}\frac{\cosh(\nu_x s)}{\hat{T}(w-a)}E_s\right\} \end{aligned} \qquad (B10)$$

Finally, (B9) and (B10) can be substituted into (B3) to obtain E_s in terms of J^a:

$$E_s = \frac{\sinh(\nu_x(w-a))}{\sinh(\nu_x(w-s))}\frac{J^a}{\Gamma_a}\cos(\alpha-\beta) \qquad (B11)$$

where

$$\Gamma_a = \frac{\Gamma_s}{\cosh(\nu_x s)} + i\nu_\beta^2\frac{\cosh(\nu_x w)}{\nu_x\sinh(\nu_x(w-s))} \qquad (B12)$$

It is now possible to use the same equations in the reverse order to determine all the unknowns coefficients used to represent the field in vacuum. In particular, Eqs (B4) and Eq. (13) give the fields at the plasma edge. At the antenna we need explicitly only the electric field along the conductors, wich is given by

$$E_y^a\cos\alpha - E_z^a\sin\alpha = \frac{\sinh(\nu_x(w-a))}{\sinh(\nu_x(w-s))}\left\{E_s\cos(\alpha-\beta) + \frac{i}{\nu_x}\sinh(\nu_x(a-s))J^a\right\} \qquad (B13)$$

The complex radiation resistance of the antenna is therefore

$$R_a + iX_a = \frac{4\pi^2 Ra}{I_a^2} \sum_{n_y} \sum_{n_z} \left(\frac{\sinh(\nu_x(w-a))}{\sinh(\nu_x(w-s))} \right)^2 |J^a|^2 \cdot \cdot \left\{ \frac{\cosh(\nu_x s)}{\Gamma_a} \cos^2(\alpha - \beta) + i\nu_x^{-1} \sinh(\nu_x(w-a)) \right\} \tag{B14}$$

where I_a is the total antenna current. Note that the vacuum field at the plasma boundary and the radiated power vanish if $\alpha - \beta = \pi/2$, i.e. if the conductors of the Faraday screen and the antenna are parallel to each other: in this case the whole field is trapped between the wall and the screen, and no coupling to the plasma is possible; more generally, Eq. (B14) shows that the Faraday shield acts as a polarising filter.

The radiation resistance can alternatively be expressed in terms of the power flux at the plasma edge:

$$R_a = \frac{4\pi^2 Ra}{I_a^2} \sum_{n_y} \sum_{n_z} \left\{ Z_{11} |B_z(0)|^2 - Z_{22} |B_y(0)|^2 + 2Z_{12} \, \mathrm{Re}\left[B_y(0) B_z^*(0) \right] \right\} \tag{B15}$$

where we have taken into account that $Z_{12} = -Z_{21}$. The equality between (B15) and the real part of (B14) must actually hold separately for each term in the sums.

b) Without Faraday shield. The expressions (3) for the fields will in this case be valid up to the antenna, $x = -a$, so that:

$$\begin{aligned} E_y^a &= \cosh(\nu_x a) \left(E_y^b + i\nu_x^2 \hat{T}(a) B_z^b \right) \\ E_z^a &= \cosh(\nu_x a) \left(E_z^b - i\nu_x^2 \hat{T}(a) B_y^b \right) \end{aligned} \tag{B16}$$

For the magnetic field we find on the plasma side:

$$\begin{aligned} B_z(a_p) &= \cosh(\nu_x a) \left[B_z(0) - i\hat{T}(a) \left((1 - n_z^2) E_y^b + n_y n_z E_y^b \right) \right] \\ B_y(a_p) &= \cosh(\nu_x a) \left[B_y(0) + i\hat{T}(a) \left(n_y n_z E_y^b + (1 - n_y^2) E_y^b \right) \right] \end{aligned} \tag{B17}$$

and on the wall side:

$$\begin{aligned} B_z(a_w) &= + \frac{i}{\nu_x^2 \hat{T}(w-a)} \left((1 - n_z^2) E_y^a + n_y n_z E_y^a \right) = \\ &= - \frac{\cosh(\nu_x a)}{\hat{T}(w-a)} \left[\hat{T}(a) B_z(0) - i\nu_x^{-2} \left((1 - n_z^2) E_y^b + n_y n_z E_y^b \right) \right] \\ B_y(a_w) &= + \frac{i}{\nu_x^2 \hat{T}(w-a)} \left(n_y n_z E_y^a + (1 - n_y^2) E_y^a \right) = \\ &= + \frac{\cosh(\nu_x a)}{\hat{T}(w-a)} \left[\hat{T}(a) B_y(0) + i\nu_x^{-2} \left(n_y n_z E_y^b + (1 - n_y^2) E_y^b \right) \right] \end{aligned} \tag{B18}$$

The jump conditions at the antenna can therefore be written:

$$
\begin{aligned}
J^a \cos\alpha &\equiv B_z(a_p) - B_z(a_w) = \\
&= \frac{\sinh(\nu_x w)}{\sinh(\nu_x(w-a))}\left[B_z(0) - \frac{i}{\nu_x^2 \hat{T}(w)}\left((1-n_z^2)E_y^b + n_y n_z E_y^b\right)\right] \\
J^a \sin\alpha &\equiv B_y(a_p) - B_y(a_w) = \\
&= \frac{\sinh(\nu_x w)}{\sinh(\nu_x(w-a))}\left[B_y(0) + \frac{i}{\nu_x^2 \hat{T}(w)}\left(n_y n_z E_y^b + (1-n_y^2)E_y^b\right)\right]
\end{aligned}
\tag{B19}
$$

Using here the boundary conditions at the plasma edge, one is led to define

$$
\begin{aligned}
Z_{11}^a &= (1-n_z^2)Z_{11} + n_y n_z Z_{21} + i\nu_x^2 \hat{T}(a) \\
Z_{12}^a &= (1-n_z^2)Z_{12} + n_y n_z Z_{22} \\
Z_{21}^a &= n_y n_z Z_{11} + (1-n_y^2)Z_{22} \\
Z_{22}^a &= (1-n_z^2)Z_{12} + (1-n_y^2)Z_{22} - i\nu_x^2 \hat{T}(a)
\end{aligned}
\tag{B20}
$$

and

$$
\Delta_a = Z_{11}^a Z_{22}^a - Z_{12}^a Z_{21}^a \tag{B21}
$$

The fields at the plasma edge are then given by

$$
\begin{aligned}
B_y(0) &= +i\frac{\nu_x \sinh(\nu_x w - a)}{\Delta_a \cosh(\nu_x w)}\left(Z_{22}^a \cos\alpha + Z_{12}^a \sin\alpha\right) J^a \\
B_z(0) &= -i\frac{\nu_x \sinh(\nu_x w - a)}{\Delta_a \cosh(\nu_x w)}\left(Z_{11}^a \sin\alpha + Z_{21}^a \cos\alpha\right) J^a
\end{aligned}
\tag{B22}
$$

Finally to evaluate the antenna resistance we obtain:

$$
\begin{aligned}
E_y^a \cos\alpha - E_z^a \sin\alpha \quad &= \quad \cosh(\nu_x a)\cdot \\
\Big\{ \Big[\Big(&(Z_{11} + i(1-n_y^2)\hat{T}(a)\Big)\cos\alpha - \Big((Z_{21} - in_y n_z \hat{T}(a)\Big)\sin\alpha\Big] B_z(0) + \\
+ \Big[\Big(&(Z_{12} + in_y n_z \hat{T}(a)\Big)\cos\alpha - \Big((Z_{22} - i(1-n_y^2)\hat{T}(a)\Big)\sin\alpha\Big] B_y(0)\Big\}
\end{aligned}
\tag{B23}
$$

Eq. (B15) for the power flux at the plasma edge holds unchanged.

Appendix C - Numerical integration.

The starting point for the FE discretisation is the Galerkin variational formulation of Eqs. (15). After an appropriate integration by parts, it can be written:

$$
\begin{aligned}
&\int_0^X dx\Big\{\Big[\Big(\frac{d}{dx}-n_y\Big)F_x^*\Big]\sigma\Big[\Big(\frac{d}{dx}-n_y\Big)(E_x+iE_y)\Big]+ \\
&\qquad F_x^*\Big[i\Big(n_y\frac{dE_y}{dx}+DE_y\Big)+(n_y^2+n_z^2-S)E_x+in_z\frac{dE_z}{dx}\Big]\Big\}= \\
&= \quad F_x^*\Big\{\sigma\Big(\frac{d}{dx}-n_y\Big)(E_x+iE_y)\Big\}_0^X \\
&\int_0^X dx\Big\{-i\Big[\Big(\frac{d}{dx}-n_y\Big)F_y^*\Big]\sigma\Big[\Big(\frac{d}{dx}-n_y\Big)(E_x+iE_y)\Big]+ \\
&\qquad \frac{dF_y^*}{dx}\Big(\frac{dE_y}{dx}+n_yE_y\Big)+F_y^*\Big[-iDE_x+(n_z^2-S)E_y+-n_yn_zE_z\Big]\Big\}= \\
&= \quad F_y^*\Big\{-i\sigma\Big(\frac{d}{dx}-n_y\Big)(E_x+iE_y)+\Big(\frac{dE_y}{dx}-in_yE_x\Big)\Big\}_0^X \\
&\int_0^X dx\Big\{\frac{dF_z^*}{dx}\Big(\frac{dE_z}{dx}-in_zE_x\Big)+F_z^*\Big[-n_yn_zE_y+(n_y^2-P)E_z\Big]\Big\}= \\
&= \quad F_z^*\Big(\frac{dE_z}{dx}-in_zE_x\Big)_0^X
\end{aligned}
\qquad (C1)
$$

where X is the high density point at which the radiation conditions (24)-(25) have to be imposed. It is required that these equations hold for all $\vec{F}$ belonging to a suitable test function vector space. Note that if $\vec{F}=\vec{E}$, the power balance equation (20) is recovered: indeed, the integration by parts is performed with this goal in mind.

Cubic Hermite interpolating functions [24] are used to implement the discretisation of Eqs. (C1). By ensuring the continuity of both the dependent functions and of their derivatives at each mesh point, these elements are particularly well suited to the solution of system of second order differential equations of the wave type, and provide fast convergence and excellent accuracy.

The Hermite interpolating functions, ψ_ν, are defined on the master interval $-1 \leq \xi \leq +1$ as:

$$\psi_0(\xi)=(|\xi|-1)^2(2|\xi|+1) \qquad \psi_1(\xi)=(|\xi|-1)^2\xi \qquad (C2)$$

Let $(x_i, \quad i=1,...,N)$ be the mesh points. Then

$$E_\alpha(x)=\sum_i\sum_{\nu=0}^{1}E_\alpha^\nu(i)F_{i,\nu}(\xi_i) \qquad (C3)$$

where

$$\begin{aligned} \xi_i &= (x - x_i)/(x_{i+1} - x_i) \qquad \text{if} \quad x_i \le x \le x_{i+1} \\ &= (x - x_i)/(x_i - x_{i-1}) \qquad \text{if} \quad x_{i-1} \le x \le x_i \end{aligned} \tag{C4}$$

and the two basic functions $F_{i,\nu}$ associated to each mesh point are defined in terms of the Hermite functions (C3) as

$$\begin{aligned} F_{i,0}(\xi_i) &= \psi_0(\xi) \qquad\qquad (-1 \le xi \le 1) \\ F_{i,1}(\xi_i) &= (x_{i+1} - x_i)\psi_1(\xi) \qquad (0 \le \xi \le 1) \\ &= (x_i - x_{i-1})\psi_1(\xi) \qquad (-1 \le \xi \le 0) \end{aligned} \tag{C5}$$

within each element, and vanish outside it. With this normalisations, $E_{\alpha,0}(i)$ and $E_{\alpha,1}(i)$ are the values of E_α and of its first derivative at $x = x_i$.

By identifying F_α in Eq. (C1) in turn with each of the basis functions used in (C3), a linear algebraic system with block tridiagonal matrix is obtained for the mesh values $E_{\alpha,\nu}$:

$$\sum_{r=-1}^{+1} \sum_{\beta=0}^{1} \mathbf{M}_{\alpha,\beta}(i, i+r) \cdot \vec{E}_\beta(i+r) = \vec{V}_\alpha(i) \tag{C6}$$

To evaluate the stiffness matrix $\mathbf{M}$ explicitly, let

$$\begin{aligned} \mathbf{Q}_i(\psi_\alpha \psi_\beta) = \int_{x_i}^{x_{i+1}} dx \Big\{ &\mathbf{\Gamma}(0,0)\psi_\alpha\psi_\beta + \mathbf{\Gamma}(0,1)\psi_\alpha \frac{d\psi_\beta}{dx} + \\ &+ \mathbf{\Gamma}(1,0)\frac{d\psi_\alpha}{dx}\psi_\beta + \mathbf{\Gamma}(1,1)\frac{d\psi_\alpha}{dx}\frac{d\psi_\beta}{dx} \Big\} \end{aligned} \tag{C7}$$

be the appropriate integrals over the element i ($x_i \le x \le x_{i+1}$). Then $\mathbf{M}$ can be constructed by making the following attributions:

$$\begin{aligned} \mathbf{Q}_i(\psi_\alpha(\xi), \psi_\beta(\xi)) &\Rightarrow \mathbf{M}_{\alpha,\beta}(i,i) \\ \mathbf{Q}_i(\psi_\alpha(\xi), \psi_\beta(-1+\xi)) &\Rightarrow \mathbf{M}_{\alpha,\beta}(i,i+1) \\ \mathbf{Q}_i(\psi_\alpha(-1+\xi), \psi_\beta(\xi)) &\Rightarrow \mathbf{M}_{\alpha,\beta}(i+1,i) \\ \mathbf{Q}_i(\psi_\alpha(-1+\xi), \psi_\beta(-1+\xi)) &\Rightarrow \mathbf{M}_{\alpha,\beta}(i+1,i+1) \end{aligned} \tag{C8}$$

(diagonal blocks get two contributions, out of diagonal only one). The non-zero coeffi-

cients in Eq. (C7) can be esily read from Eq. (C1):

$$
\begin{aligned}
&\mathbf{\Gamma}_{x,x}(0,0) = n_y^2 + n_z^2 - S + \sigma n_y^2 \\
&\mathbf{\Gamma}_{x,x}(0,1) = \mathbf{\Gamma}_{x,x}(1,0) = -\sigma n_y \\
&\mathbf{\Gamma}_{x,x}(1,1) = \sigma \\
&\mathbf{\Gamma}_{x,y}(0,0) = -\mathbf{\Gamma}_{y,x}(0,0) = i(\sigma n_y^2 + D) \\
&\mathbf{\Gamma}_{x,y}(0,1) = -\mathbf{\Gamma}_{y,x}(1,0) = i(1-\sigma) n_y \\
&\mathbf{\Gamma}_{x,y}(1,1) = -\mathbf{\Gamma}_{y,x}(1,1) = i\sigma \\
&\mathbf{\Gamma}_{x,z}(0,1) = -\mathbf{\Gamma}_{z,x}(1,0) = i n_z \\
&\mathbf{\Gamma}_{y,y}(0,0) = n_z^2 - S + \sigma n_y^2 \\
&\mathbf{\Gamma}_{y,y}(0,1) = \mathbf{\Gamma}_{y,y}(1,0) = -\sigma n_y \\
&\mathbf{\Gamma}_{y,y}(1,1) = 1 + \sigma \\
&\mathbf{\Gamma}_{y,z}(0,0) = \mathbf{\Gamma}_{z,y}(0,0) = -n_y n_z \\
&\mathbf{\Gamma}_{z,z}(0,0) = n_y^2 - P \\
&\mathbf{\Gamma}_{z,z}(1,1) = 1
\end{aligned}
\qquad (C10)
$$

As well known, the boundary terms $\vec{V}_\alpha$ on the r.h. side eliminate each other between adiacent elements, except at the extremes $x = 0$ and $x = X$, where they are easily expressed in terms of the boundary conditions (24) to (26). In particular, $\vec{V}_\alpha(0)$ is the only non-vanishing terms on the r.h. side of the discretized system. Taking into account the properties of the Hermite interpolating functions, we find at $x = 0$:

$$
\begin{gathered}
V_{x,0}(0) = 0 \qquad V_{y,0}(0) = -iB_z \qquad V_{z,0}(0) = iB_z \\
\vec{V}_1 = 0
\end{gathered}
\qquad (C11)
$$

To impose the radiation condition (24), τ_F and τ_B have to be considered as two additional unknowns; they can easily be taken into account simply adding Eqs. (24) to the stiffness matrix.

It is perhaps worth mentioning in this context that it would be possible in principle to combine the vacuum equations (7) to (13) and the discretized equations in the plasma into a single linear system: a single inversion would then determine the solution satisfying the radiation conditions (24) *and* the jump conditions at the antenna which specify the excitation. This procedure however would couple the vacuum constants $E_y^a, \cdots, B_z^b$ directly to τ_F and τ_B, thereby irrimediably perturbing the block-tridiagonal structure of the stiffness matrix. The introduction of the surface impedance matrix, although requiring the determination of two independent solutions in the plasma instead of one only, is nevertheless advantageous also from the numerical point of view, as it makes the inversion much simpler.

References.

/1/ S. Puri, S. Tutter, Proc 2d Int. Conf. on Waves and Instabilities in Plasmas, Innsbruck 1975, paper P1.

/2/ S. Puri, Proc 3d Top. Conf. on RF Plasma Heating, Pasadena (Calif.) 1978, paper E1.

/3/ S. Puri, Phys. Fluids, **22** (1979) 1716.

/4/ M. Ono, T.H. Stix, K.L. Wong, R. Horton, 2d Joint Varenna-Grenoble Int. Symp. on Heating in Toroidal Plasmas, Como 1980, Vol 1, p. 593.

/5/ M. Ono, K.L. Wong, Phys. Rev. Lett., **45** (1980) 1105.

/6/ M. Ono, K.L. Wong, G.A. Wurden, Phys. Fluids, **26** (1983) 298.

/7/ M. Ono, G.A. Wurden, K.L. Wong, Phys. Rev. Lett., **52** (1984) 37.

/8/ M. Ono et al., Phys. Rev. Lett., **54** (1986) 2239.

/9/ M. Ono et al., 11th IAEA Int. Conf. on Plasma Phys. and Contr. Nucl. Fus. Res.,, (Kyoto 1986), paper F-I-3

/10/ T. Watari et al., 11th IAEA Int. Conf. on Plasma Phys. and Contr. Nucl. Fus. Res.,, (Kyoto 1986), paper F-I-5

/11/ T. Mutoh et al., 11th IAEA Int. Conf. on Plasma Phys. and Contr. Nucl. Fus. Res.,, (Kyoto 1986), paper D-III-2

/12/ M. Porkolab et al., 11th IAEA Int. Conf. on Plasma Phys. and Contr. Nucl. Fus. Res.,, (Kyoto 1986), paper F-II-2

/13/ Y. Takase et Al. Report PFC/JA-86-60, MIT 1986 (Submitted to Phys. Rev. Lett.).

/14/ M. Ono, Ion Bernstein Wave Heating, Theory and Experiment, in Proc. Course and Workshop on Applications of RF Waves to Tokamak Plasmas, Varenna 1985, p. 197.

/15/ S. Puri, Phys. Fluids, **26** (1983) 164.

/16/ F. Skiff, M. Ono, P. Colestock, K.L. Wong, Phys. Fluids, **28** (1985) 2453.

/17/ W. N.-C. Sy, T. Amano, R. Ando, A. Fukuyama, T. Watari, Nucl. Fusion, **25** (1985) 795.

/18/ J. Adam et al, Proc. 4th Top. Conf. on RF Plasma Heating, Austin 1981, paper A1.

/19/ A. Messiaen et al, Proc. 3d Varenna-Grenoble Int. Symp. on Heating in Toroidal Plasmas, Grenoble 1982, Vol. 1 p. 243.

/20/ V.P. Bhatnagar et al, Nucl. Fusion, **22** (1982) 280.

/21/ A. Ram, A. Bers, Nucl. Fusion, **24** (1984) 679.

/22/ K. Teilhaber, J. Jacquinot, Nucl. Fusion, **24** (1984) 541.

/23/ P. Lallia, Nucl. Fusion, **15** (1975) 1190.

/24/ K. Appert et al., Comp. Phys. Comm. **40** (1986) 73.

/25/ D.G. Swanson, Proc. 3d Joint Varenna-Grenoble Int. Symp. on Heating in Toroidal Plasmas1982, Vol 1, p. 285.

/26/ P.L. Colestock, R.J. Kashuba, Nucl. Fusion, **23** (1983) 763.

/27/ M. Brambilla, M. Ottaviani Plasma Phys. Contr. Fusion, **27** (1985) 919.

/28/ T.H. Stix, *The Theory of Plasma Waves*, McGraw-Hill (N.Y.) 1961.

/29/ M. Brambilla, M. Ottaviani, Plasma Phys. Contr. Fusion**27** (1985) 1.

/30/ B.D. Fried, , S.D. Conte, *The plasma dispersion function,* Academic Press, N.Y. 1961.

/31/ R.R. Weynants, Phys. Rev. Lett., **33** (1974) 78.

/32/ M. Brambilla, Report IPP-4/209, Garching 1982.

/33/ F. Skiff, M. Ono, K.L. Wong, Phys. Fluids **27** (1984) 1051.

/34/ V.E. Golant, Sov. Phys. Tech. Phys. 16 (1972) 1980.

/35/ K. Steinmetz et al., 11th IAEA Int. Conf. on Plasma Phys. and Contr. Nucl. Fus. Res.,, (Kyoto 1986), paper F-I-2.

Table 1

Standard Alcator C parameters.

Torus radius	64 cm
Plasma radius	12 cm
Magnetic field on axis	6.5 to 8 Tesla
Central electron density	$1.0\ 10^{14}$ cm^{-3}
Limiter electron density	$0.6\ 10^{13}$ cm^{-3}
Central electron temperature	1.5 keV
Limiter electron temperature	0.050 keV
Plasma composition	100% Hydrogen
Central ion temperature	0.2 B_o - 0.5 keV
Limiter ion temperature	0.050 keV
Width of the scrape-off plasma	0.5 cm
Density e-folding length	0.25 cm
Temperature e-folding length	1.4 cm
Applied frequency	183.6 Mhz
Single T-antenna (central feeder, short at the ends)	
Effective propag. constant $\sqrt{LC}$	1.73
Width of the antenna conductor	1.6 cm
Half length of the antenna	12.5 cm
Distance antenna-wall	3.8 cm
Distance antenna-Faraday shield	1.1 cm
Distance Faraday shield-plasma	0 cm

Figure Captions.

Fig. 1. - Antenna geometry for Bernstein wave coupling.

Fig. 2 - Antenna and Faraday shield seen from the plasma, arbitrary orientation of the conductors. For BW coupling $\alpha = \beta = 90°$.

Fig. 3 - Radiation resistance versus ω/Ω_{ci} at the limiter radius (for this and all the following figures the plasma and antenna parameters are those of Table 1, unless explicitly otherwise stated).

Fig. 4 - Fraction of power in the various channels versus ω/Ω_{ci} at the limiter radius.

Fig. 5 - Power radiated in the various channels versus ω/Ω_{ci} at the limiter radius, at constant antenna current (arb. units; the power in the Fast Wave and in the electrons have been multiplied by 10 for clarity).

Fig. 6 - $\omega/\Omega_{ci} = 2.02$ at the limiter radius. a) n_z spectre (normalised to unity); b) power deposition profile (W/cm^{-3} per MW); c), d) Electric field components (kV/cm at 1 MW).

Fig. 7 - $\omega/\Omega_{ci} = 1.99$ at the limiter radius. a) n_z spectre (normalised to unity); b) power deposition profile (W/cm^{-3} per MW); c), d) Electric field components (kV/cm at 1 MW).

Fig. 8 - $\omega/\Omega_{ci} = 1.96$ at the limiter radius. a) n_z spectre (normalised to unity); b) power deposition profile (W/cm^{-3} per MW); c), d) Electric field components (kV/cm at 1 MW).

Fig. 9 - n_z spectre of a dipole antenna of the same dimensions as the standard one; $\omega/\Omega_{ci} = 1.96$ at the limiter radius.

Fig. 10 - Radiation resistance versus scrape-off thichness, keeping the values of n_e and $T_{e,i}$ at the limiter radius and their e-folding lengths constant.

Fig. 11 - Radiation resistance versus density e-folding length, keeping the values of n_e and $T_{e,i}$ at the limiter radius and the scrape-off thickness constant.

Fig. 12 - Radiation resistance versus scrape-off thichness, keeping the values of n_e and $T_{e,i}$ at the limiter radius constant, but varyying the e-folding lengths so that n_e and $T_{i,e}$ at the Faraday screen are also constant.

Fig. 13 - Radiation resistance versus edge temperature. Scrape-off thickness and e-folding lengths as in the standard case.

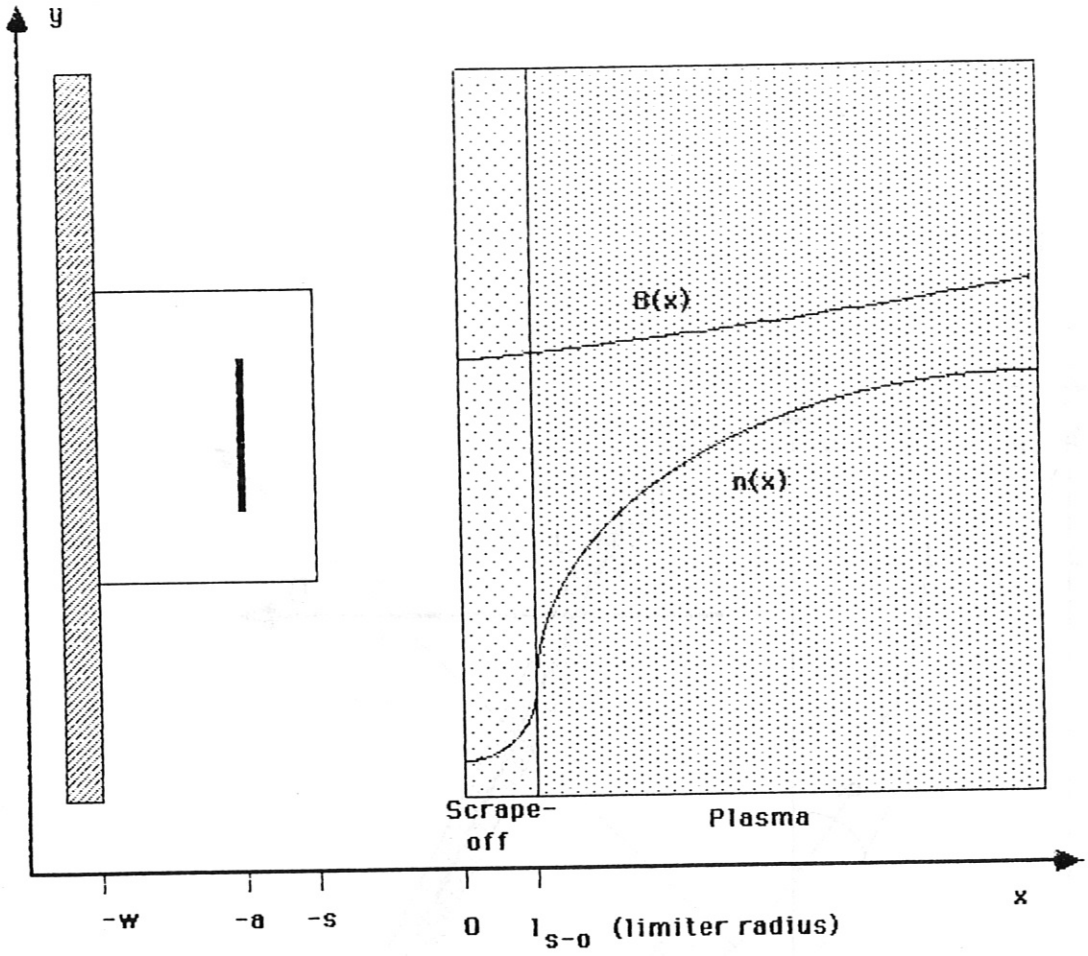

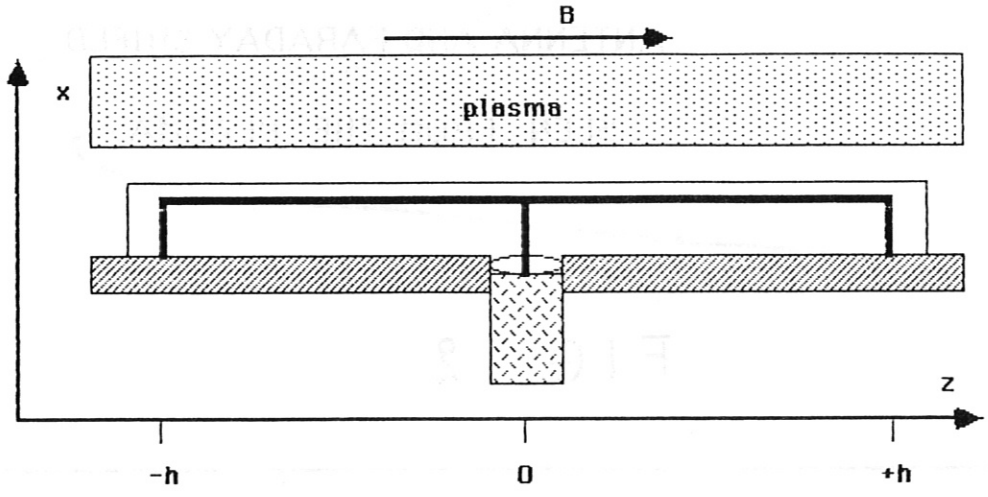

ANTENNA GEOMETRY

FIG. 1

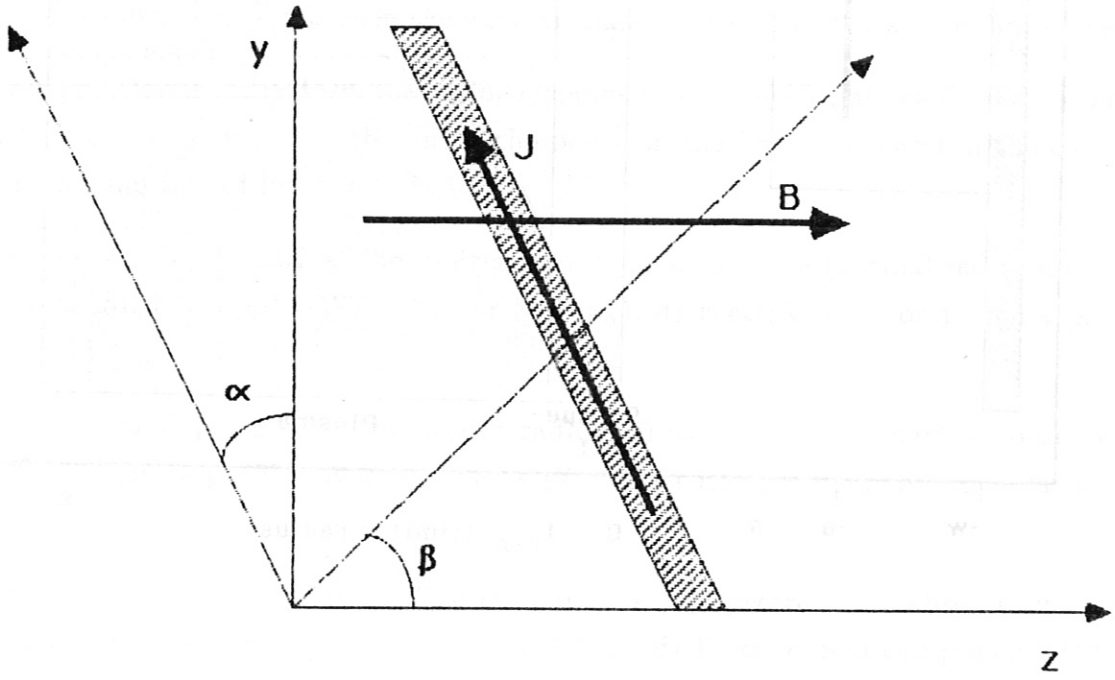

ANTENNA AND FARADAY SHIELD

SEEN FROM THE PLASMA

FIG. 2

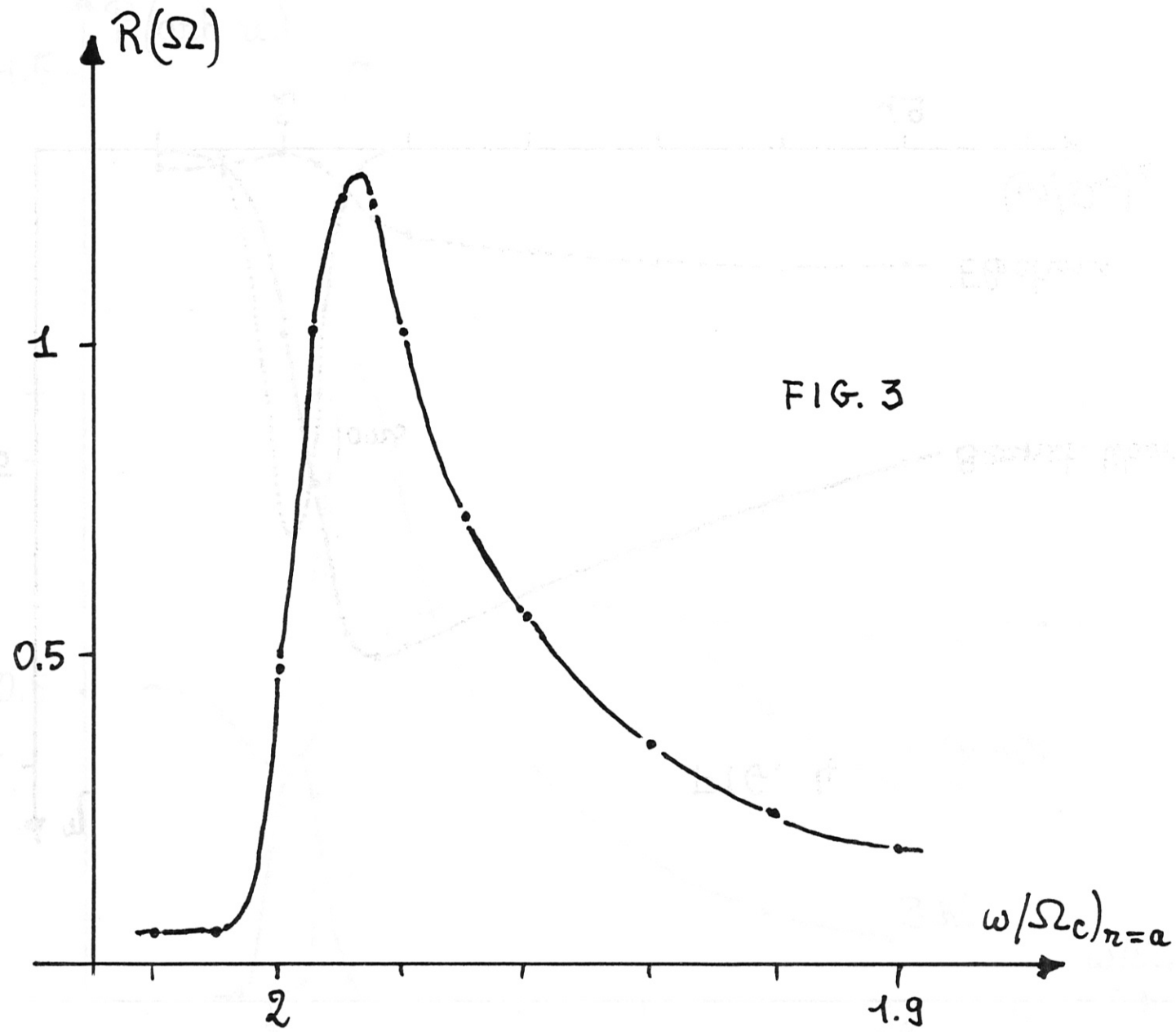

FIG. 3

FIG. 4

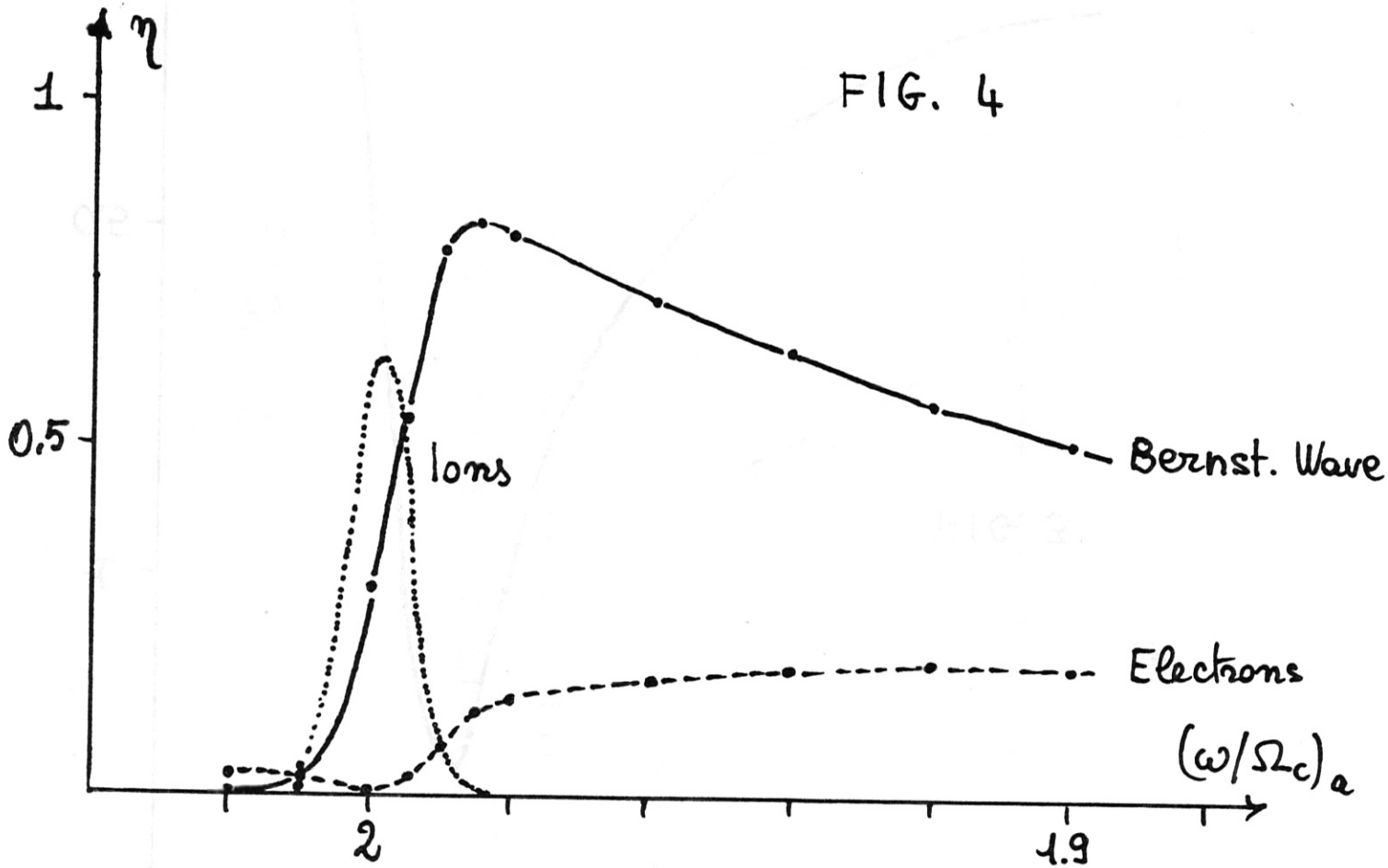

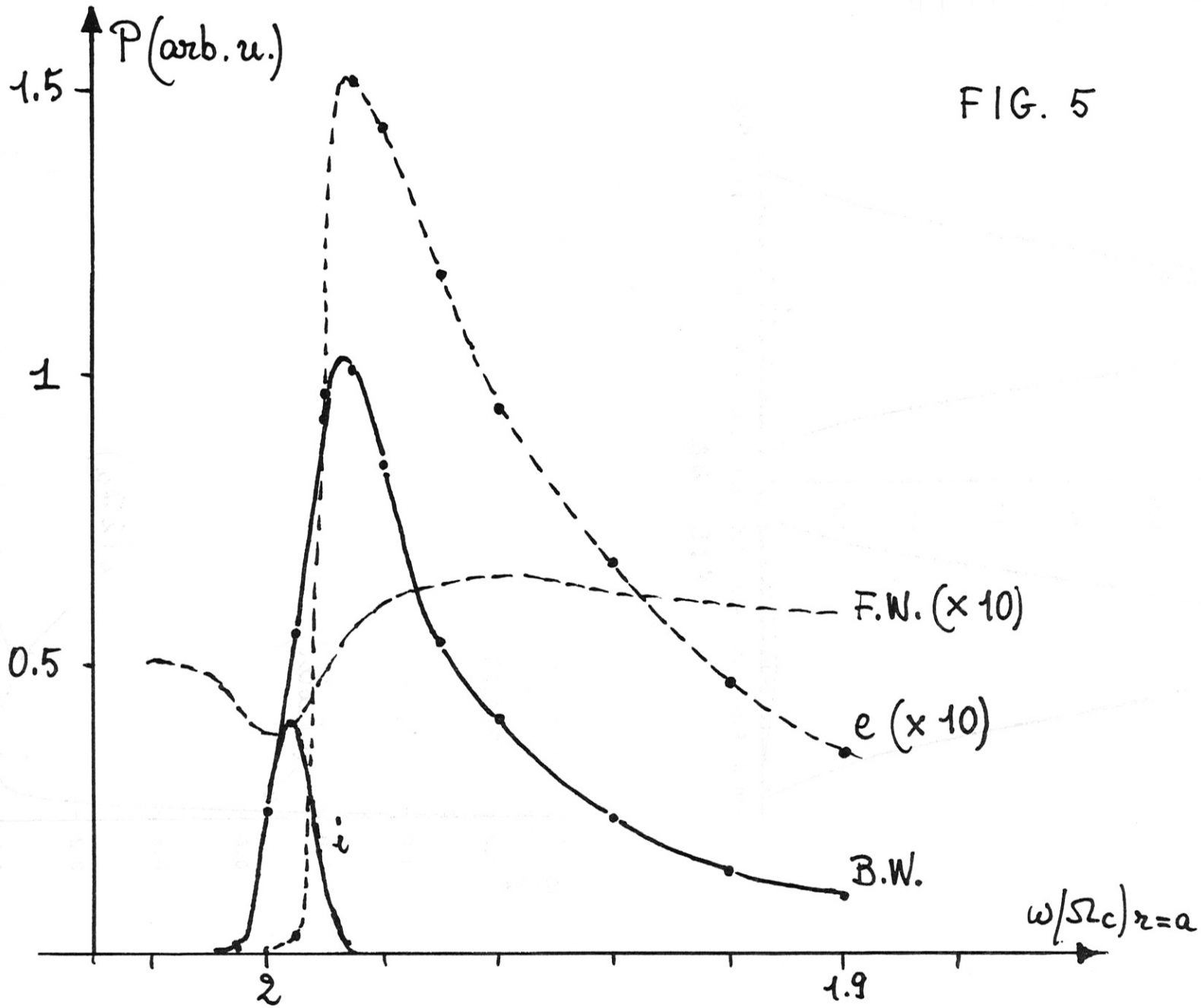

FIG. 5

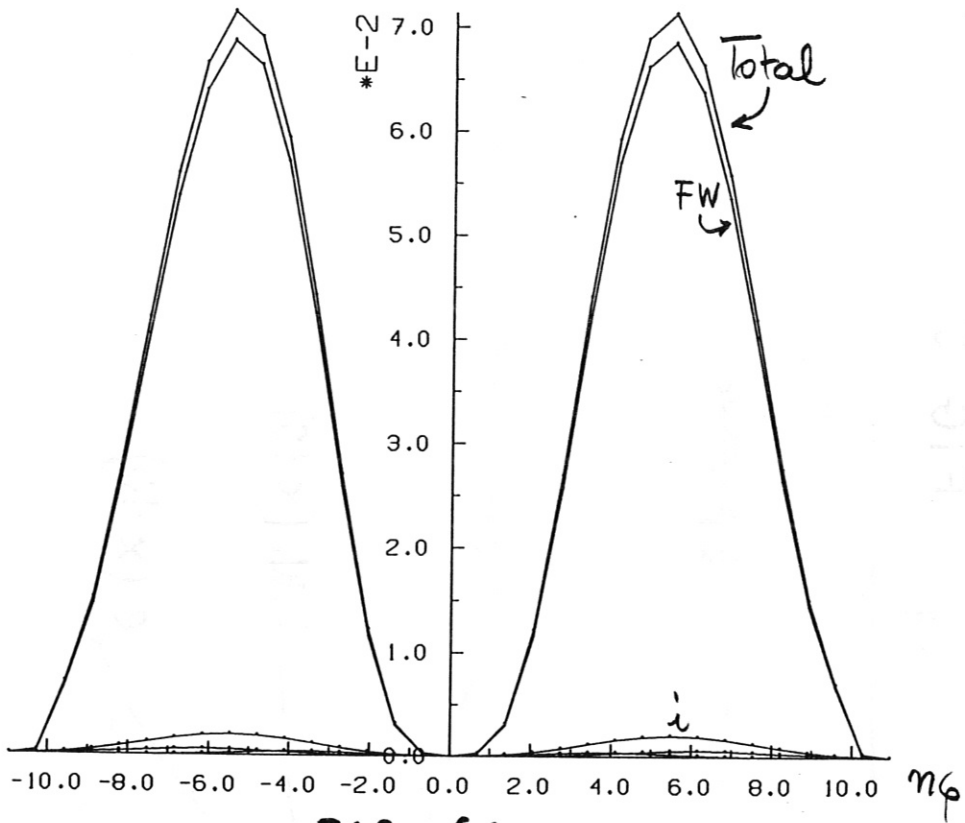
*E-2
7.0
6.0
5.0
4.0
3.0
2.0
1.0
0.0
Total
FW
i
-10.0 -8.0 -6.0 -4.0 -2.0 0.0 2.0 4.0 6.0 8.0 10.0
nφ

FIG. 6a

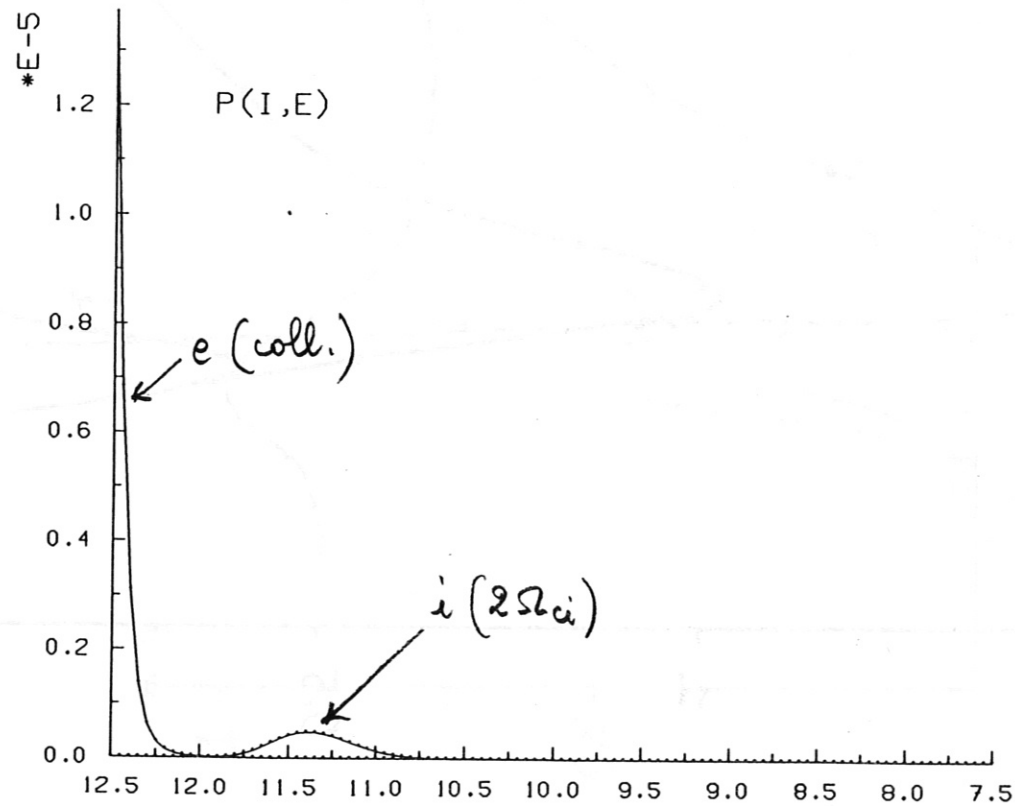
*E-5
P(I,E)
1.2
1.0
0.8
0.6
0.4
0.2
0.0
e (coll.)
i (2Ωci)
12.5 12.0 11.5 11.0 10.5 10.0 9.5 9.0 8.5 8.0 7.5

FIG. 6b

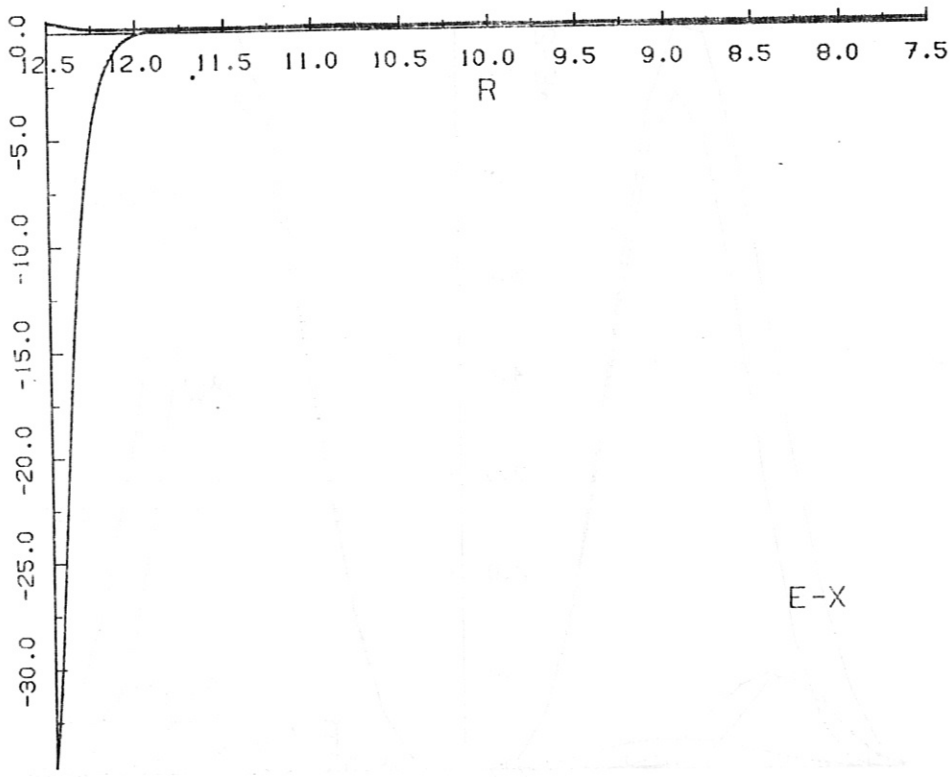
0.0
-5.0
-10.0
-15.0
-20.0
-25.0
-30.0
12.5
12.0
11.5
11.0
10.5
10.0
9.5
9.0
8.5
8.0
7.5
R
E-X

FIG. 6c

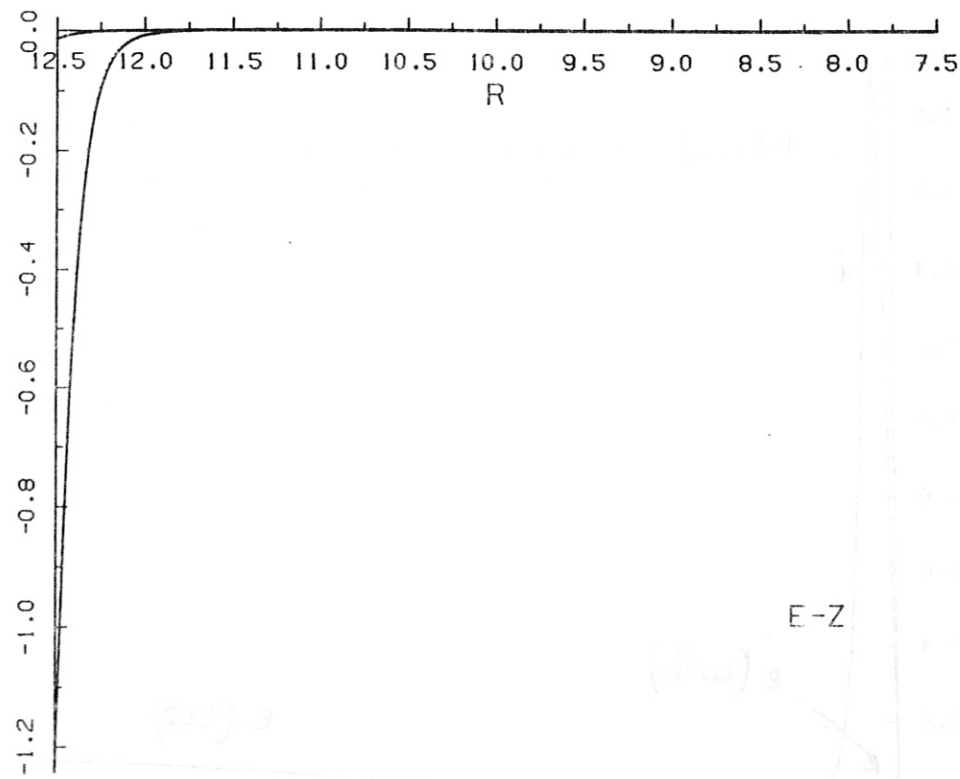
0.0
-0.2
-0.4
-0.6
-0.8
-1.0
-1.2
12.5
12.0
11.5
11.0
10.5
10.0
9.5
9.0
8.5
8.0
7.5
R
E-Z

FIG. 6d

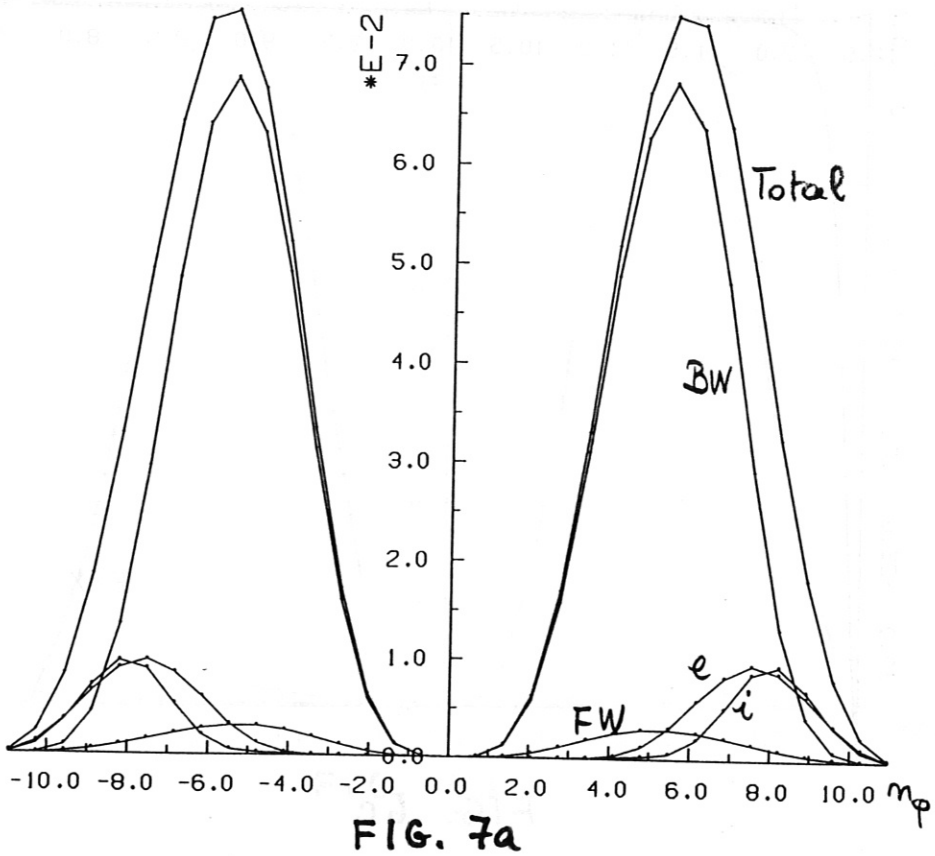
*E-2
7.0
6.0
5.0
4.0
3.0
2.0
1.0
0.0
Total
BW
FW
e
i
-10.0 -8.0 -6.0 -4.0 -2.0 0.0 2.0 4.0 6.0 8.0 10.0
η_φ

FIG. 7a

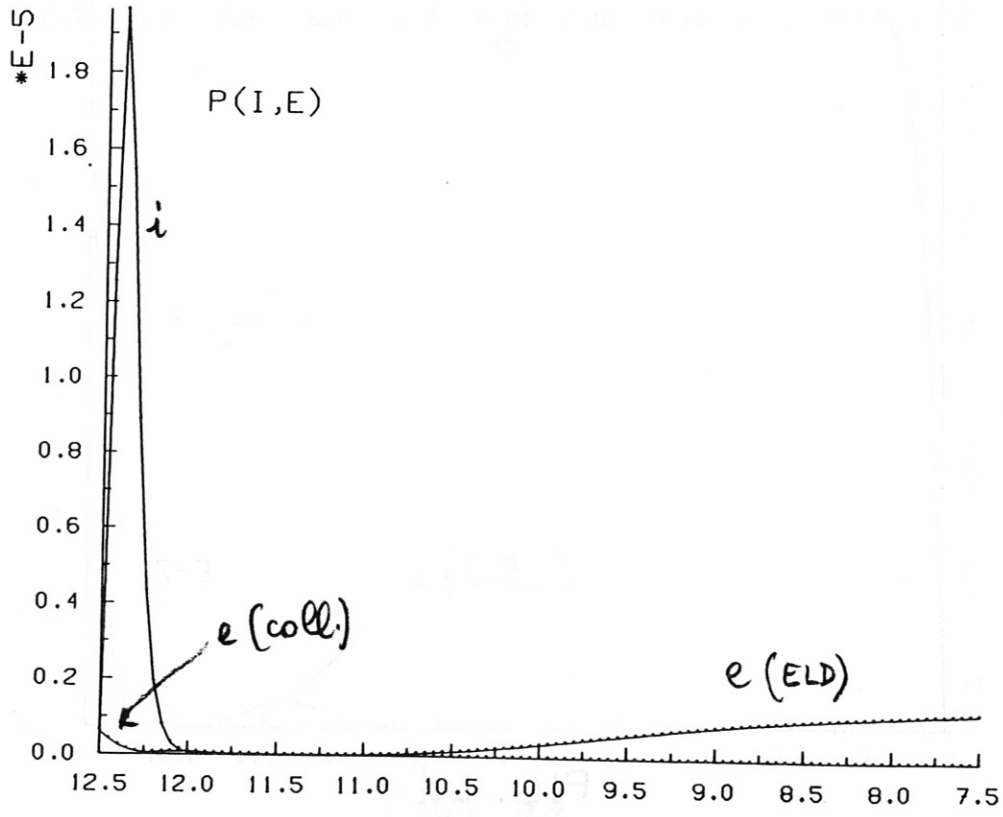
*E-5
1.8
1.6
1.4
1.2
1.0
0.8
0.6
0.4
0.2
0.0
P(I,E)
i
e (coll.)
e (ELD)
12.5 12.0 11.5 11.0 10.5 10.0 9.5 9.0 8.5 8.0 7.5

FIG. 7b

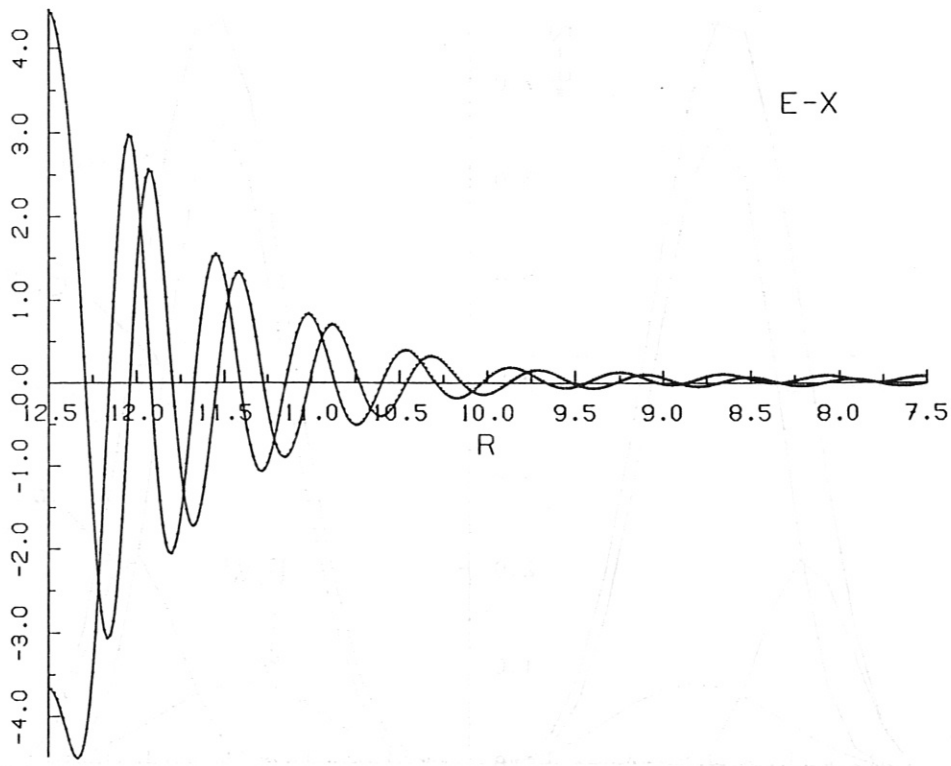
E-X
4.0
3.0
2.0
1.0
0.0
-1.0
-2.0
-3.0
-4.0
12.5
12.0
11.5
11.0
10.5
10.0
9.5
9.0
8.5
8.0
7.5
R

FIG. 7c

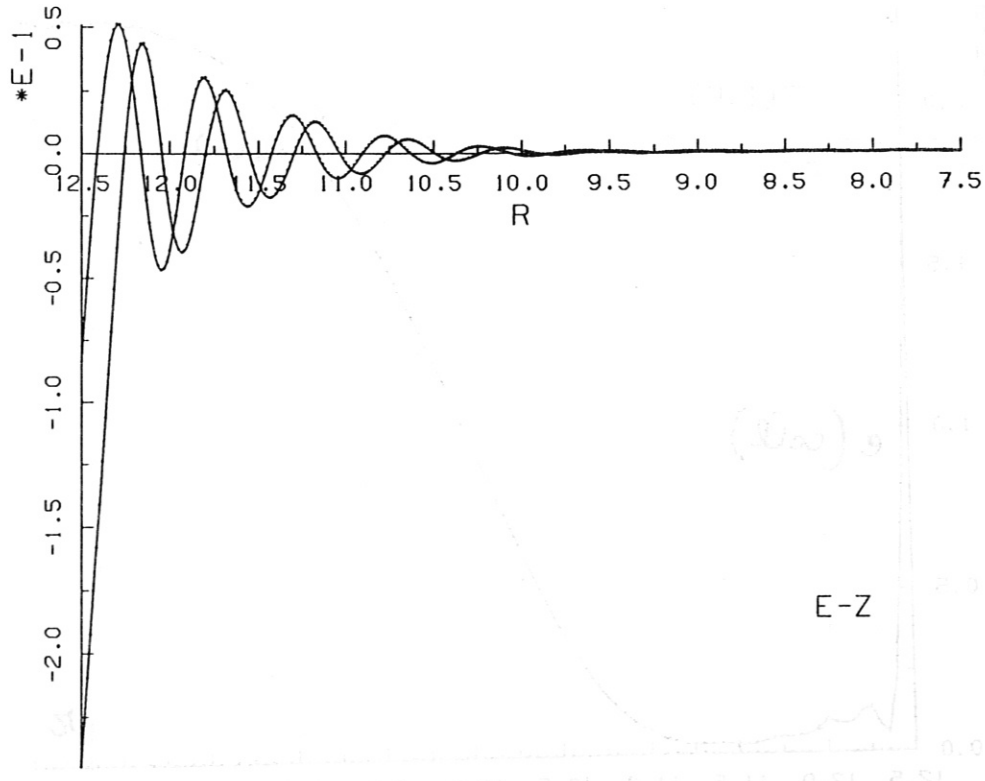
*E-1
0.5
0.0
-0.5
-1.0
-1.5
-2.0
12.5
12.0
11.5
11.0
10.5
10.0
9.5
9.0
8.5
8.0
7.5
R
E-Z

FIG. 7d

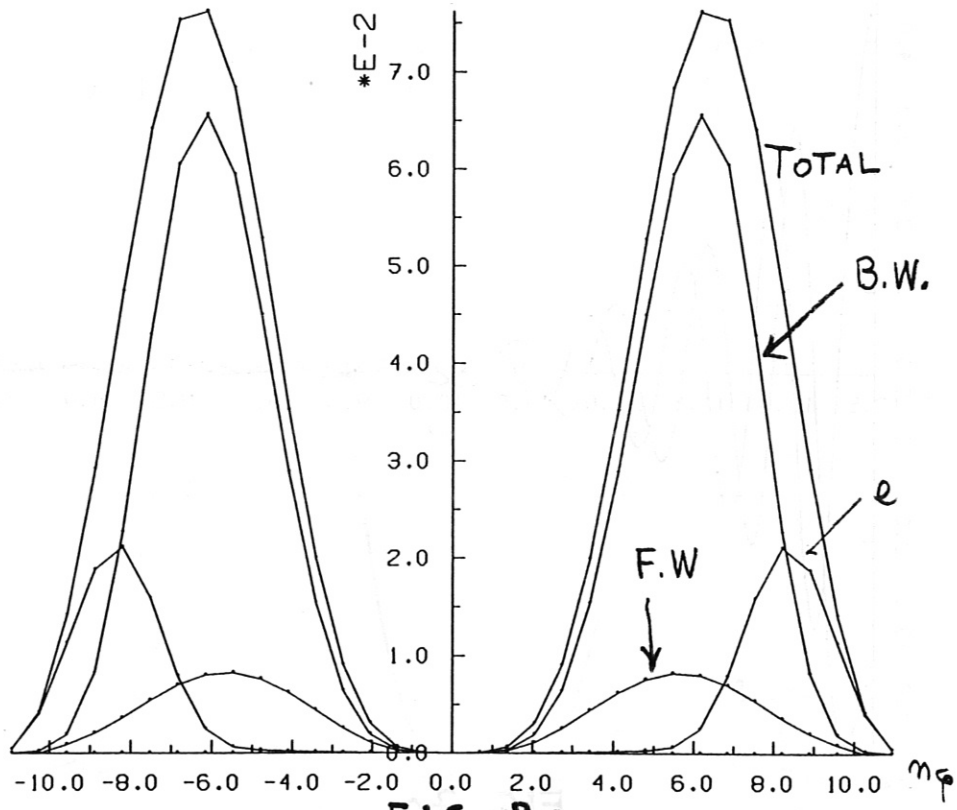
*E-2
7.0
6.0
5.0
4.0
3.0
2.0
1.0
0.0
TOTAL
B.W.
e
F.W
-10.0 -8.0 -6.0 -4.0 -2.0 0.0 2.0 4.0 6.0 8.0 10.0
nφ

FIG. 8a

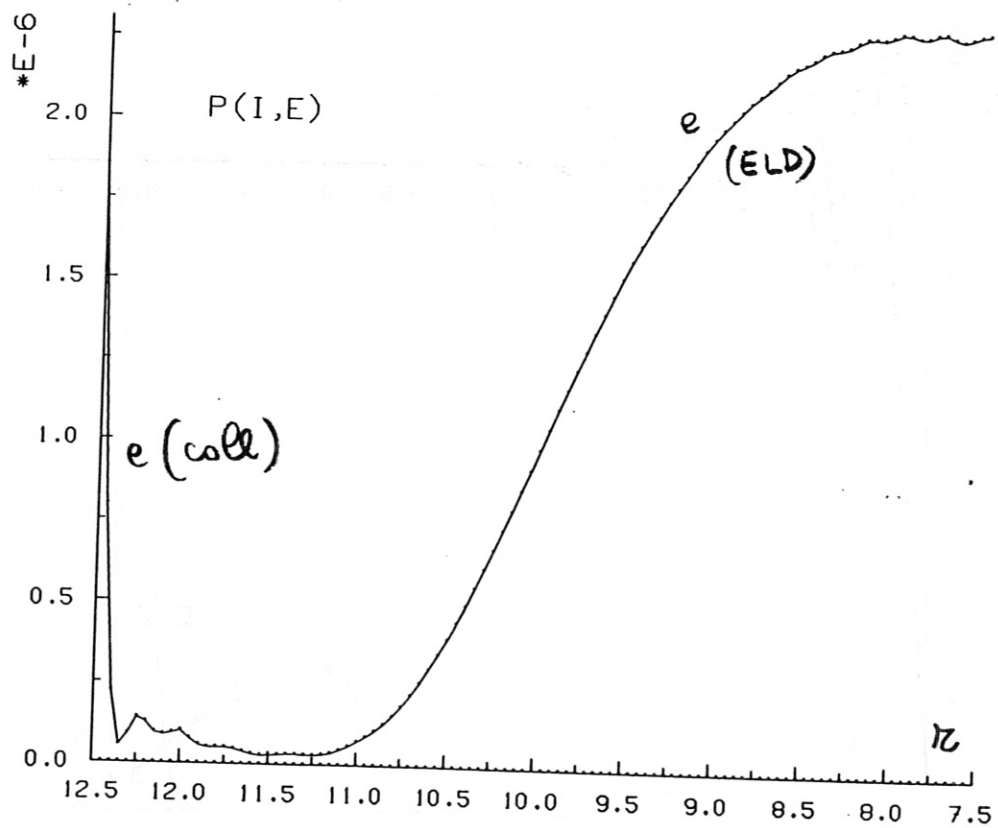
*E-6
2.0
1.5
1.0
0.5
0.0
P(I,E)
e
(ELD)
e (coll)
12.5 12.0 11.5 11.0 10.5 10.0 9.5 9.0 8.5 8.0 7.5
R

FIG. 8b

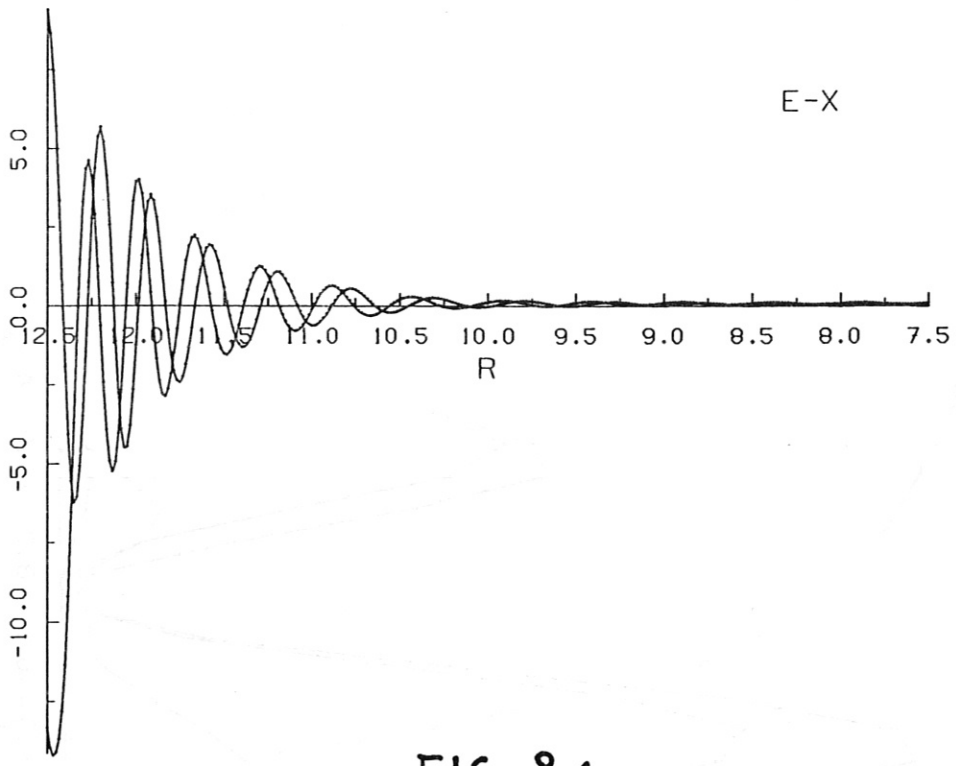
E-X
5.0
0.0
-5.0
-10.0
12.5
12.0
11.5
11.0
10.5
10.0
9.5
9.0
8.5
8.0
7.5
R

FIG. 8c

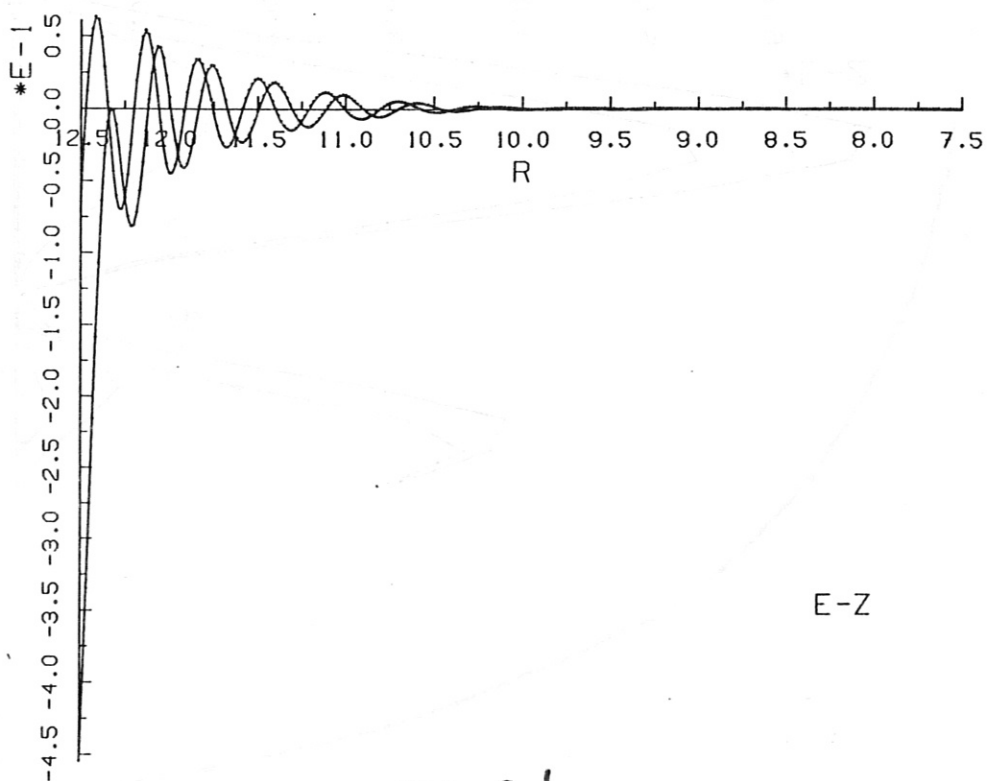
*E-1
0.5
0.0
-0.5
-1.0
-1.5
-2.0
-2.5
-3.0
-3.5
-4.0
-4.5
12.5
12.0
11.5
11.0
10.5
10.0
9.5
9.0
8.5
8.0
7.5
R
E-Z

FIG. 8d

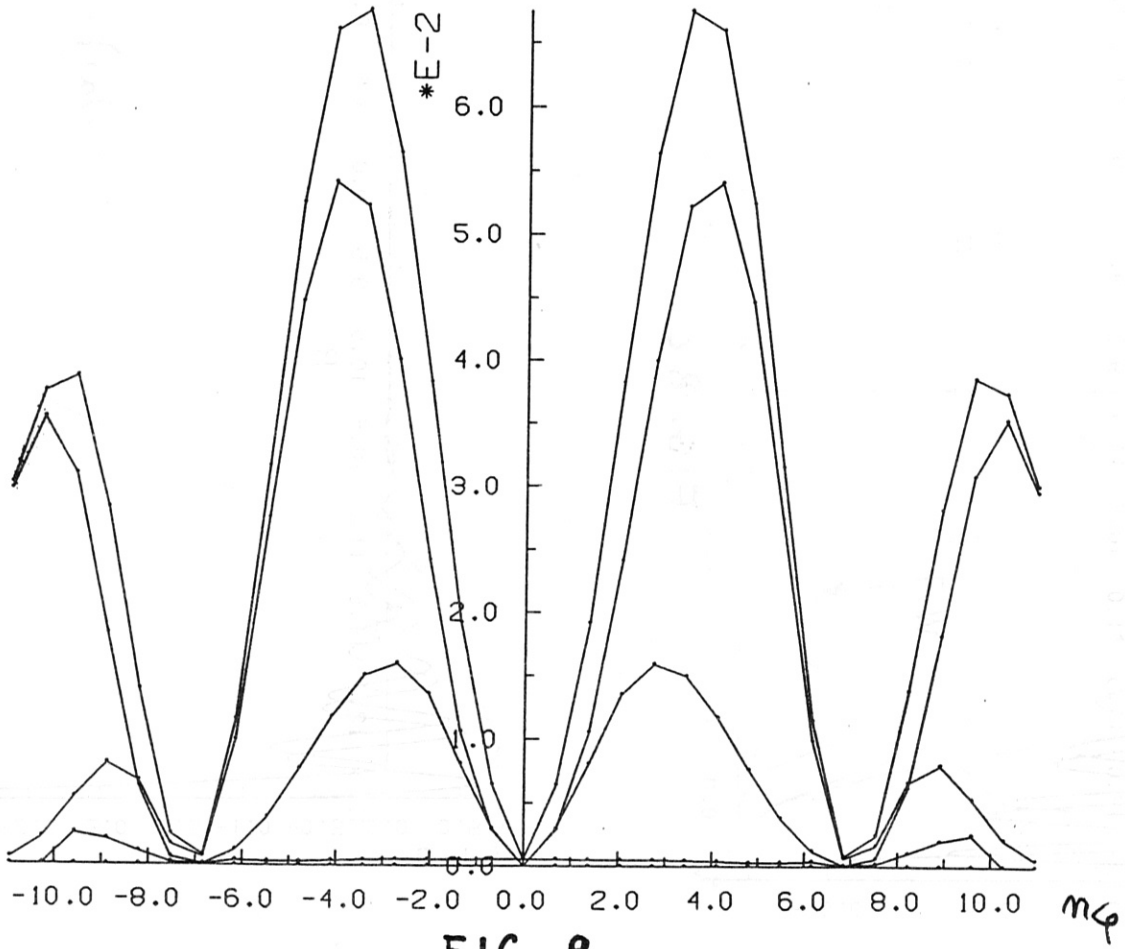

FIG. 9

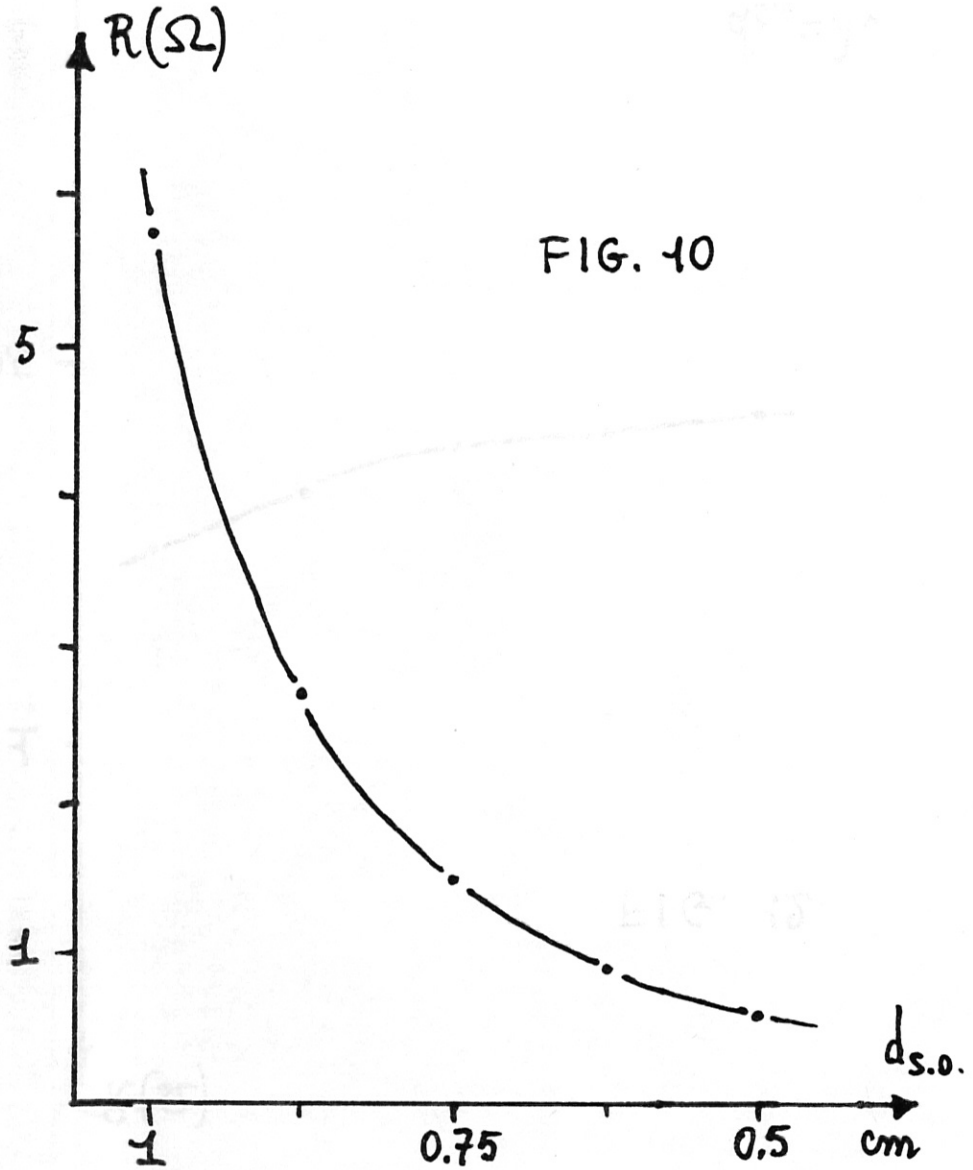

FIG. 10

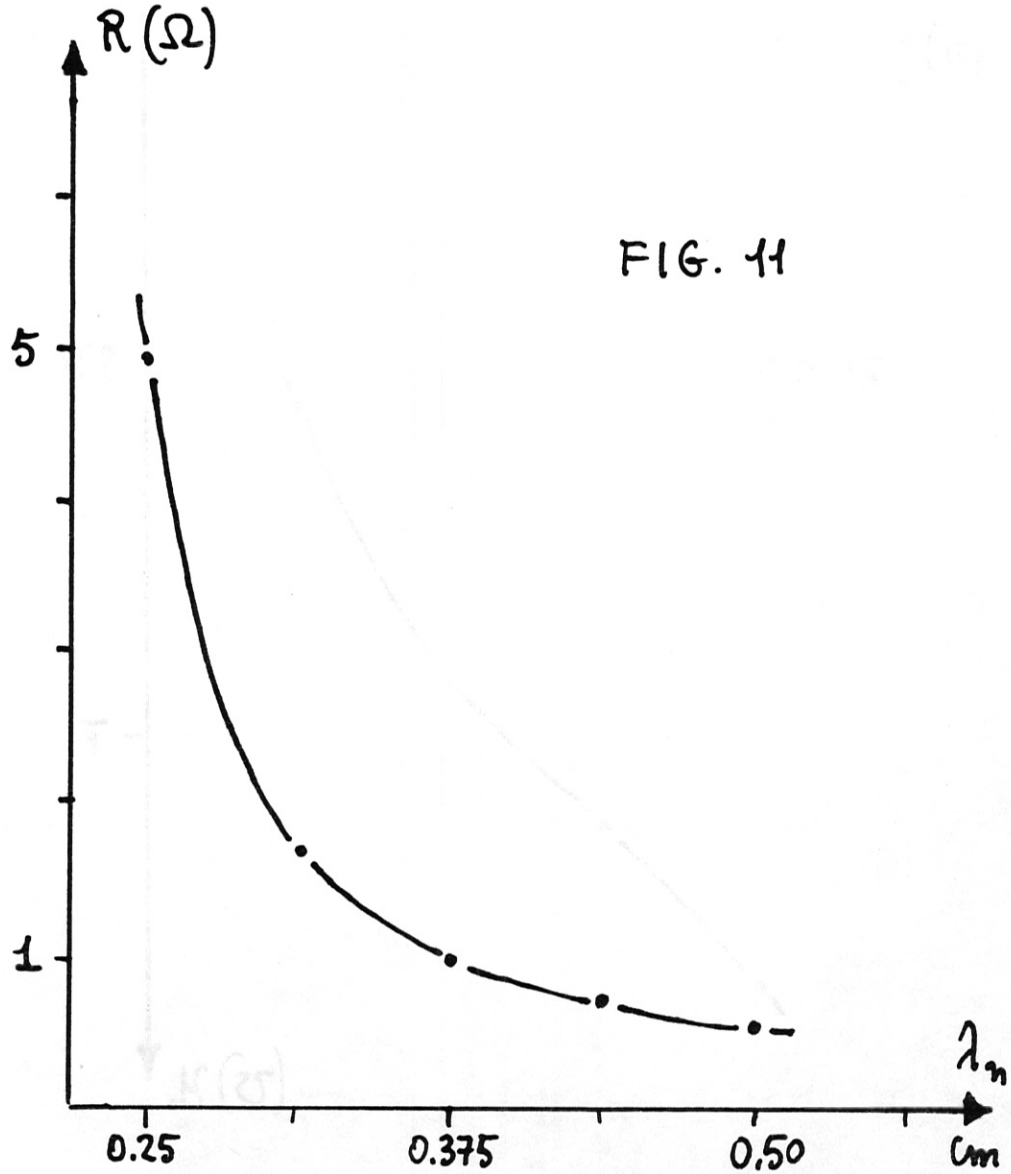

FIG. 11

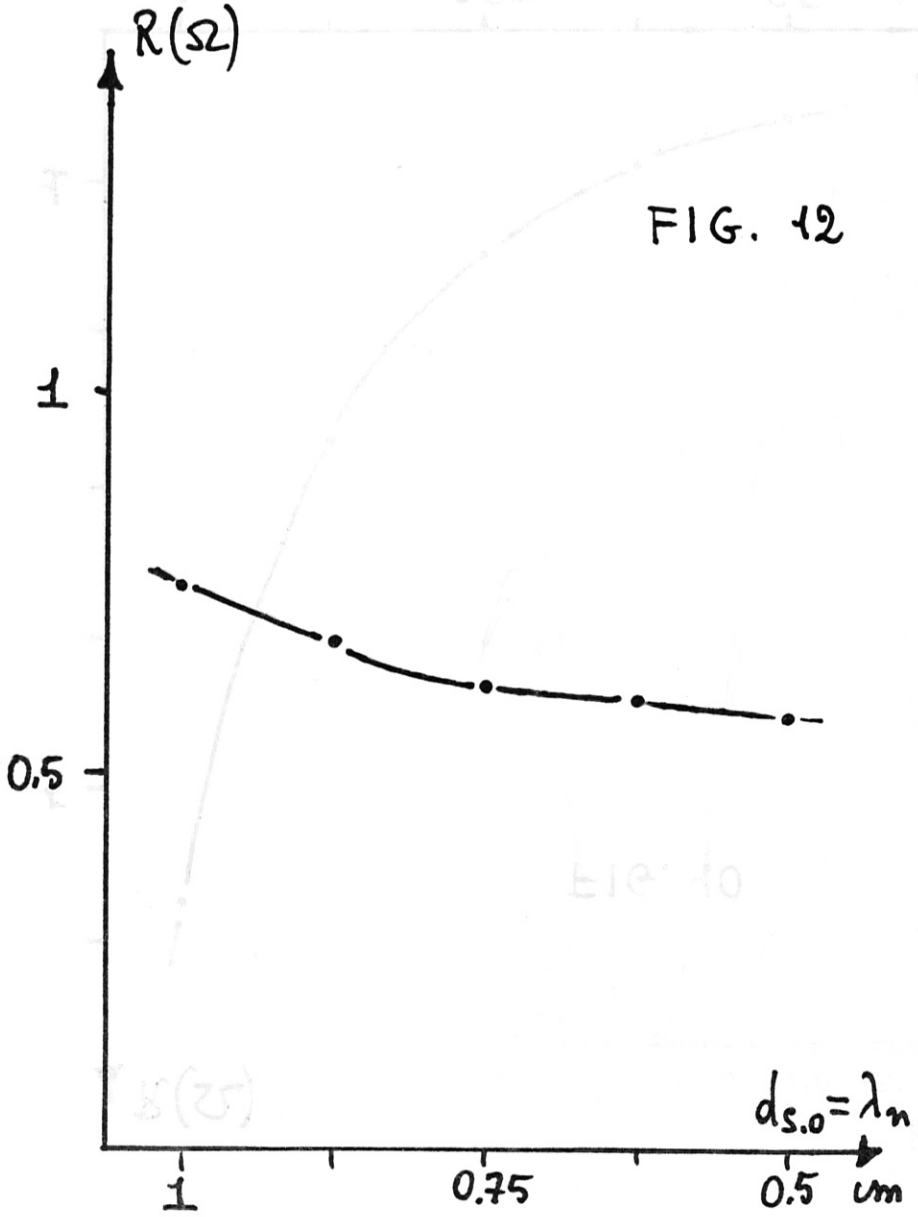

FIG. 12

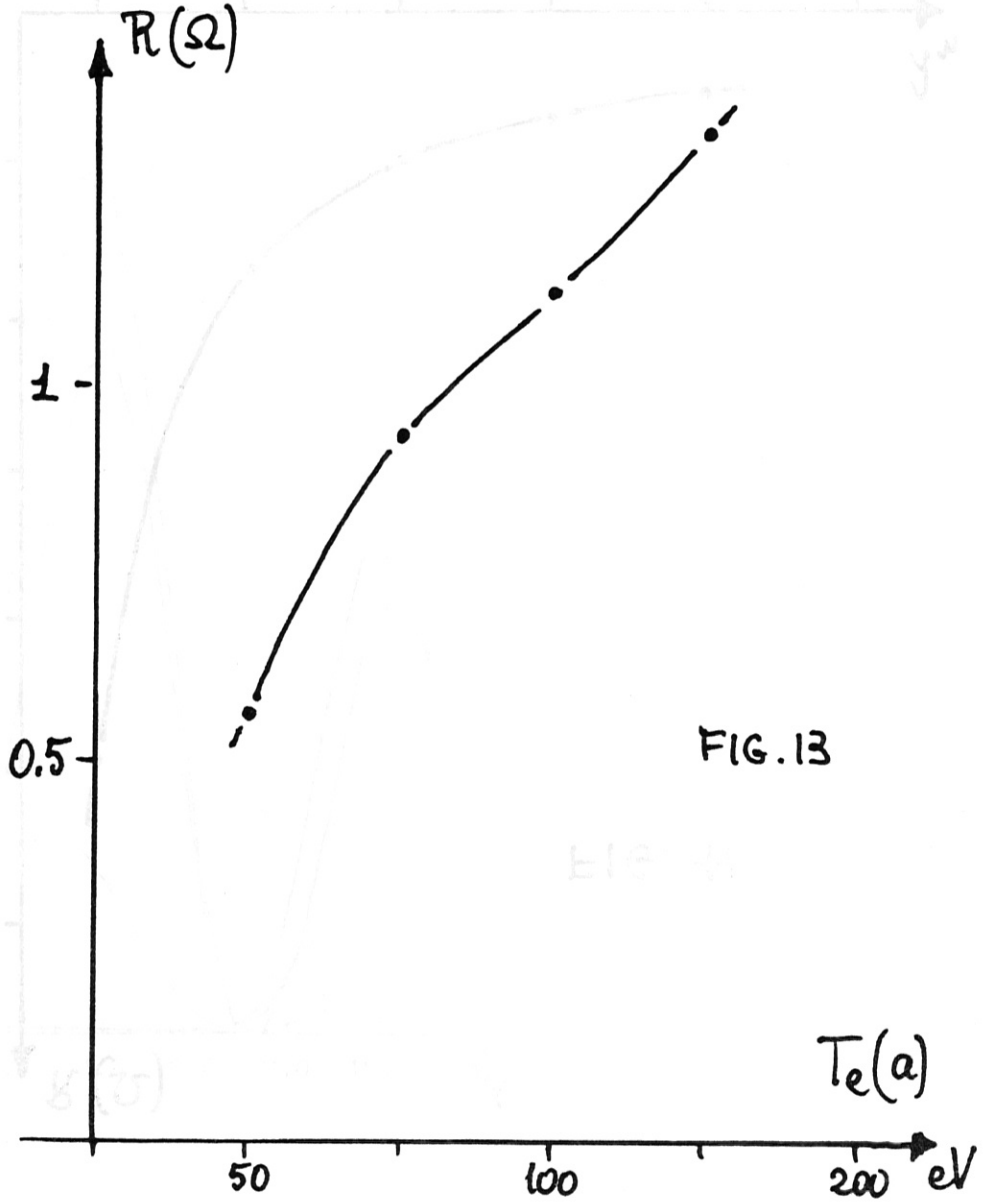

FIG. 13